NTNU

Norwegian University of
Science and Technology

Modelling of Multistream LNG Heat Exchangers

Joan Soler Fossas

Natural Gas Technology
Submission date: June 2011
Supervisor: Kjell Kolsaker, EPT

Norwegian University of Science and Technology
Department of Energy and Process Engineering

Abstract

The main goal of this thesis is to find out if a liquefied natural gas multistream heat exchanger numerical model is achievable. This should include several features usually neglected in nowadays available heat exchanger models, such as flow maldistribution, changes in fluid properties and heat exchanger dynamic behaviour. In order to accomplish that objective a simpler case is modelled. Efforts are put in achieving numerical stability.

A counter flow natural gas and mixed refrigerant heat exchanger is modelled. Some important characteristics of the obtained model are: (1) it allows a dynamic study of the heat exchanger, (2) mass flow rate is a consequence of inlet and outlet pressure difference, (3) fluid properties change is taken into account, (4) it presents a time step control function and (5) fluid movement is not neglected.

Some interesting numerical behaviours included in heat exchangers models design that have been observed during the course of this thesis are discussed. For instance, the comparison of the effects of choosing one heat transfers correlation or another.

Dynamic response of the modelled heat exchanger during start up and during an abrupt change in mixed refrigerant inlet temperature are shown and discussed.

Preface

This Master thesis was completed at the Department of Energy and Process Engineering of the Norwegian University of Science and Technology (NTNU) from February 2011 to June 2011.

First, I would like to thank my supervisor, NTNU professor Kjell Kolsaker, for his help and guidelines during the course of this Master thesis. I specially appreciate that he has always been opened to my questions and doubts, no matter the time it took to solve them.

I would also like to thank to Øivind Wilhelmsen, who belongs to SINTEF staff. His advices during all the semester helped me a lot. Specially, at the end, when his help in structuring the thesis became really valuable.

I would like to thank this country and its people, Norway and the Norwegians, for giving an all day example of the well done work.

I would also like to thank my friends, in Norway and abroad, because no thesis could give what a friendship does.

I would like to thank my parents for the excellent example that they have always been, for the unconditional love that they have always shown and for how fortunate they make me feel.

Finally, I would like to thank Núria because she always makes the things look brighter.

Table of Contents

List of figures

List of tables

Nomenclature table

A_1, A_2, A_3 Friedel's correlation constants

d_h hydraulic diameter

f friction factor

$f(\dots)$ polynomial linking function

Fr Froude number

g gravitational acceleration

G mass flux

h heat transfer coefficient

H intensive enthalpy

L length

$\dot{m}$ mass flow rate

N total cells number

P pressure

q'' heat flux

Re Reynolds number

S surface

t time

v specific volume

V volume

We Webber number

x_e thermodynamic equilibrium quality

z stream-wise coordinate

Greek symbols

α void fraction

β channel aspect ratio

λ thermal conductivity

μ viscosity

ρ density

σ surface tension

ϕ two phase pressure drop multiplier

Superscripts

$\bar{}$ two phase

k time step

Subscripts

a accelerational

c contraction

e expansion

f fluid

g saturated vapour

i cell position

in channel inlet

l saturated liquid

lam laminar flow

lo liquid only

out channel outlet

S Shell

sp single phase

t tube

tot total

tp two phase

$trans$ transitional flow

tur turbulent flow

w wall

1 Background and objective

1.1 Introduction

There are a lot of situations where natural gas transportation by pipeline is overly expensive. One of the most common ways to transport the gas in these situations is to liquefy it.

Since the combined-cycle turbine power plants are getting more and more common, the Liquefied Natural Gas (LNG) demand will keep growing. Therefore it is justified to study and develop all the necessary tools to reduce the cost, both operational and capital, of a LNG plant.

LNG projects are inherently capital-intensive, with the liquefaction process representing the 50% of total project cost [1] as shown in figure 1. The liquefier is the key area where a process designer can make largest cost savings and influence the project viability.

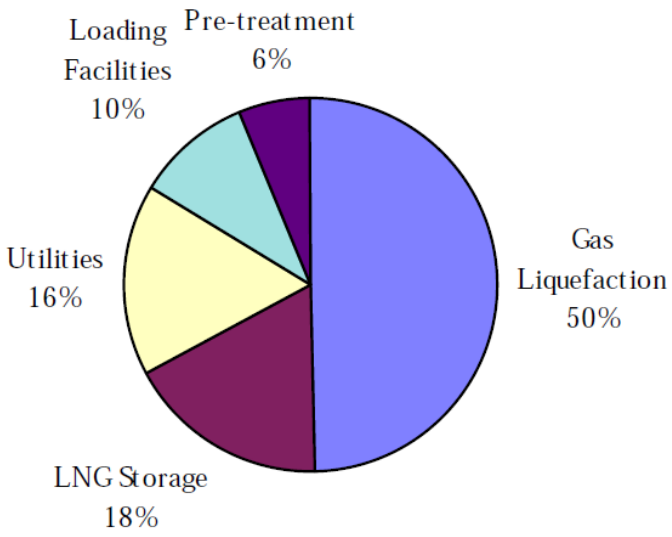

Figure 1 - Typical Breakdown of Liquefaction Plant Capital Cost [1]

In the liquefaction process the most important elements are the heat exchangers. These rule the behaviour of the process and restrict the production and efficiency of the plant in every situation.

Due to their safe and cost-effective designs and the need for higher effectiveness and efficiency, MultiStream Heat Exchangers (MSHE) are preferred rather than the normal two stream heat exchangers in many energy-intensive industrial and cryogenic processes. Natural gas liquefaction is one of them.

A multistream heat exchanger is a single unit in which multiple hot and cold streams exchange heat simultaneously. Plate & fin, spiral wound and multipass shell and tube are the most common types of MSHEs. This thesis refers to a multipass shell and tube MSHE, which

is the result of hundreds of thin shell and two tubes working in parallel. Usually, a low pressure refrigerant such as a pure or multicomponent refrigerant flows down the shell side. The tube side is occupied by the hot streams; usually each stream fills one tube.

Heat exchangers are the main components in cryogenic processes. In LNG plants they represent 20-30% of the investment cost [2, 3]. In addition, their performance affects the sizing and design of other equipment, namely compressors and their power drivers.

It has been studied by several authors how thermodynamic considerations make cryogenic processes very sensitive to the HE performance [2, 4, 5].

A cryogenic HE in a LNG plant is expected to have an efficiency higher than 90%. This means that the design has to be really accurate and it has been noticed that several effects that are neglected when designing a high-temperature HE should not be neglected when designing a HE for cryogenic applications.

These non-negligible effects are: changes in fluid properties, flow maldistribution, longitudinal thermal conduction and heat-in-leakage. The consideration of this effects depend on the effectiveness that a HE is expected to perform:

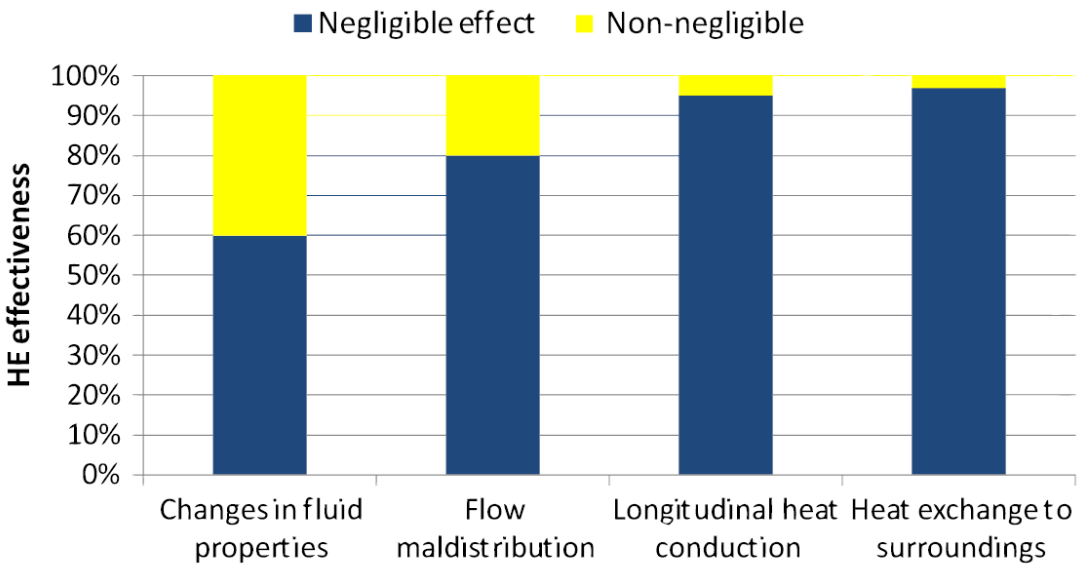

Figure 2 - Several typical assumptions impact on the HE design depending on the HE effectiveness [2]

Thus, as it has been explained MSHEs play an important role in the operation and the design of a LNG plant. It is the engineer's priority to find the way to improve their design and to predict their performance. Therefore lots of heat exchangers simulations models have been developed in the last decades and are used extensively for both designing plants and evaluating the actual performance of a plant.

However, over the last years it has been seen that there is a need to improve HE models for cryogenic applications. This is specially the case when it comes to reducing the number of

assumptions of ideal conditions that are used. One of the reasons is the pursuing of more energy, cost and space efficient plants. Features used to achieve this include among others mixed refrigerant and more compact heat exchangers. These features will in many cases lead to conditions where ideal assumptions are no longer valid. If this is not taken into account when designing the plant, it could give operational challenges and as well lead to an energy consumption that is higher than anticipated.

Because of its own nature, MSHEs with phase change involve several physical phenomena that should be considered when modelling them.

Characteristics it is important to account for in the design phase include:

- Distribution of two phase fluids into several parallel channels.
- Instabilities in channels with evaporation/condensation.
- Maldistribution of two phase fluids within heat exchangers channels.
- Two phase non equilibrium conditions (both thermodynamic and fluid dynamic effects like slip).
- Heat exchanger dynamic behaviour, for instance at start up and shut down.

Both steady state and dynamic heat exchanger models are widely used in the design processes of heat exchangers and overall LNG production plants. Detailed plant operability analysis requires good dynamic heat exchanger models. As the plant complexity increases, it is seen that these kind of analysis are important parts of the plant process as well.

The heat exchanger models which are used are usually based on enthalpy balance calculations or on heat transfer and pressure drop correlations. The latter method is normally more detailed and geometry dependent than the first one.

The correlation based models will in addition to correlations, based on empirical results, contain some kind of assumptions in order to simplify the heat exchanger modelling. Assumptions of equal two phase distribution, stable flow conditions and thermodynamic equilibrium are common.

SINTEF Energy Research is currently running a competence building project (KMB: “Low emissions LNG systems”) with contribution from NTNU and industry partners, focusing on both fundamental physics, heat exchanger design and system optimisation.

This thesis aims to produce a model capable of including part of the problematic here explained. The goal is to produce a tool that allows improved LNG process designs.

1.2 Aim of the thesis

The objective of this thesis is to find out if it is possible to develop a MSHE numerical model that includes most of the problematic already explained. This model should simulate a multistream heat exchanger working with natural gas. The model should be able to simulate

satisfactorily phase changes in transient conditions. Minimum simplifications as possible should be assumed in fluid properties field.

Main model characteristics that will be appreciated are numerical stability, accuracy and CPU time consumption. Specially, first one will be the most important since the other two can be improved later if a stable model is developed.

To achieve this conclusion, a simpler model will be developed. A counter flow two streams shell and tube heat exchanger will be modelled. This model should be a tool that allows a heat exchanger designer know more about the LNG process dynamics.

Efforts will be put in achieving a working numerically stable model. Experimental validity of the results is not the goal of this thesis, hence, there can be some of the used data that may not be as accurate as desired in a final heat exchanger design. Besides, the optimisation of the model can be done afterwards in further work researches.

1.3 Description of the thesis

In chapter 2 is an explanation of the preliminary concepts that are necessary to understand this thesis. Chapter 2.1 focuses on the heat exchanger, what it is, where it is used and how it is designed. Since a heat exchanger model is developed in this thesis, chapter 2.1.1 goes deeper in the design issue and the heat transfer and pressure drop correlations used in the model are explained there. Chapter 2.2 is a basic theory explanation of finite different methods and its basic concepts.

Calculations belong to chapter 3. First, in chapter 3.1, the case modelled is explained in detail. Chapter 3.2 is an explanation of the model solution methodology, the procedure to achieve the satisfactory code and its structure and operation are described in it.

Chapter 4 consists of the results and observations that are product of this thesis. In chapter 4.1 some relevant numeric characteristics that have been observed during the model development are presented and discussed. Chapter 4.2 is an illustration and discussion of the results obtained from the case of study.

Chapter 5 summarizes the most important and relevant issues that are product of this thesis.

A future work proposal is done in chapter 5.2.

2 Preliminary concepts

2.1 Heat exchangers

Shah and Sekulic give the following heat exchanger definition [6]: A heat exchanger is a device that is used for transfer of thermal energy (enthalpy) between two or more fluids, between a solid surface and a fluid, or between solid particulates and a fluid, at differing temperatures and in thermal contact, usually without external heat and work interactions.

In most heat exchangers, the fluids are separated by a heat transfer surface, and ideally do not mix. A heat exchanger consists of a heat exchanging elements such as core or a matrix containing the heat transfer surface, and fluid distribution elements such as headers, manifolds, tanks, inlet and outlet nozzles... Usually, there are no moving parts.

The heat transfer surface is a surface of the heat exchanger core that is in direct contact with fluids and through which heat is transferred by conduction.

The balance differential equation that governs the fluid enthalpy variation when the fluid is in contact with the heat transfer surface is the following:

$$\rho \partial V \frac{\partial H}{\partial t} = \dot{m} \frac{\partial H}{\partial z} + \partial q \qquad \text{Eq. (1)}$$

Where the last term in the right hand of the equation is the differential heat flow, which is defined by the next equation:

$$\partial q = h \, \partial S_{f,w} \, (T_w - T_f) \qquad \text{Eq. (2)}$$

Notice that the heat transfer coefficient is then the parameter which will define the heat exchanger volume in a design, or the one that will govern its efficiency when evaluating the HE performance.

Another important part of a HE design is the pressure drop that is caused by the fluid going through it. Pressure drop will directly define the capital and operational costs of the process where the heat exchanger is used. A fluid that suffers a high pressure drop going through a HE will provoke high costs in compressors or pumps investment and power consumption.

Thus, heat transfer and pressure drop in heat exchanger are two important features that which need a special attention of the designer. Therefore, chapter below gives a further explanation of them and of the way they have been modelled in this thesis.

2.1.1 Heat transfer and pressure drop characteristics

Heat transfer and pressure drop inside a heat exchanger are two complex phenomena that have been studied in decades. Researchers have been concerned with developing predictive models for several industries, such as traditional ones like steam and nuclear power

generation, chemical and petroleum, etc. or newer ones like electronics and all micro-channel refrigeration systems that it includes.

2.1.1.1 Two phase flow types

It is known that pressure drop and heat transfer characteristics depend strongly on two-phase flow types. Depending on mass and heat flows and on vapour fraction, apart from other variables, two-phase flow types are:

- Bubble flow: Liquid fills all the pipe while some small vapour bubbles are in a mixture with it.
- Slug flow: Big vapour bubbles travel through the pipe separated by a liquid film.
- Annular flow: Liquid covers only a thin film through the pipe wall while vapour flows through an inside channel with some droplets in it.

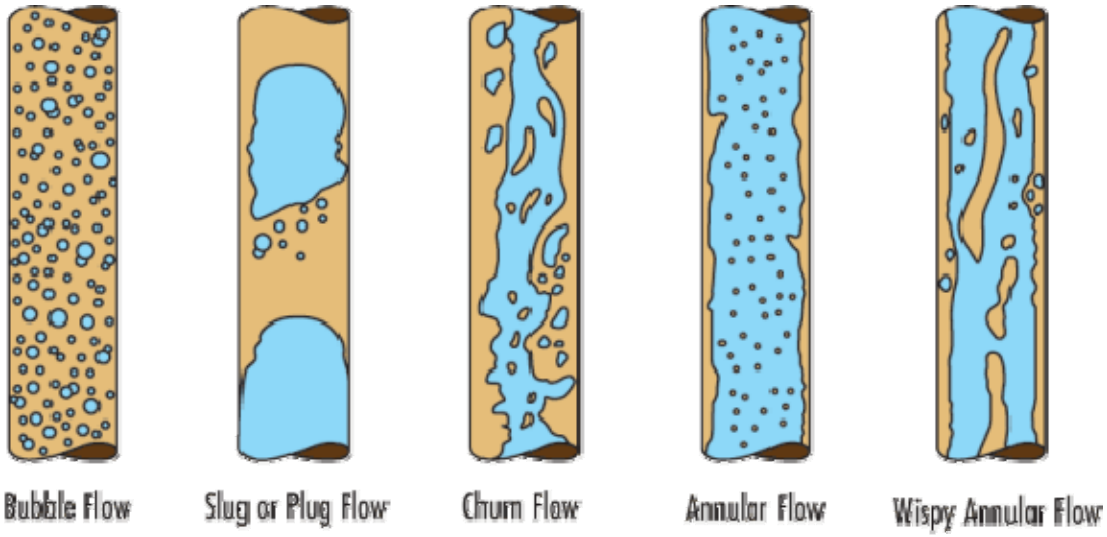

Figure 3 - Two phase flow types

In the upper figure the different flow types can be observed. Churn and wispy annular flow can be considered middle terms between slug and annular flow.

Two phase correlations described below base their calculations on the influence of each flow type when a phase change occurs.

2.1.1.2 Heat transfer

2.1.1.2.1 Single phase

Two popular single phase heat transfer coefficient correlations for turbulent flow ($Re \geq 3000$) in a pipe are the one developed by Dittus and Boelter [7] and Gnielinski [8].

Dittus and Boelter correlation is:

$$Nu = Nu_{tur} = 0.023 Re^{0.8} Pr^{0.4} \qquad \text{Eq. (3)}$$

And Gnielinski correlation is:

$$Nu = Nu_{tur} = \frac{\frac{f}{8}\,(Re - 1000)\,Pr}{1 + 12.7\sqrt{\frac{f}{8}}\,(Pr^{\frac{2}{3}} - 1)} \qquad \text{Eq. (4)}$$

$$f = (1.82\log(Re) - 1.64)^{-2} \qquad \text{Eq. (5)}$$

It is decided to use Gnielinski heat transfer correlation since it was noticed after some simulations that Dittus and Boelter correlation introduced higher numerical oscillations in the system.

Hausen [9] correlation will be the single phase laminar flow heat transfer correlation used in the model. So, for $2300 \leq Re$:

$$Nu = Nu_{lam} = 3.66 + \frac{0.0668 \cdot \frac{d_h}{L} \cdot Re \cdot Pr}{1 + 0.04 \cdot \left(\frac{d_h}{L} \cdot Re \cdot Pr\right)^{2/3}} \qquad \text{Eq. (6)}$$

If the Reynolds number is within the upper limit of Hausen correlation and the lower limit of the Gnielinski correlation, Nusselt number will be calculated as an interpolation of both to guarantee Nusselt continuity. For $2300 < Re < 3000$:

$$Nu = interpolation(Nu_{lam}(Re),\ Nu_{tur}(Re), Re) \qquad \text{Eq. (7)}$$

It is reminded that once the Nusselt number has been defined, heat transfer coefficient is found by the following equation:

$$h_{sp} = \frac{Nu \cdot \lambda_{sp}}{d_h} \qquad \text{Eq. (8)}$$

2.1.1.2.2 Two phase

2.1.1.2.2.1 Evaporation

Liu and Winterton [10] correlation is used when calculating evaporation heat transfer.

$$h_{tp} = \left(\left(Eh_{sp}\right)^2 + (Sh_{nb})^2\right)^{0.5} \qquad \text{Eq. (9)}$$

Where h_{sp} is Dittus-Boelter single phase heat transfer coefficient for the liquid (already explained), h_{nb} is the nucleate boiling coefficient:

$$h_{nb} = 55{P_r}^{0.12}\left(-\log_{10}(P_r)\right)^{-0.55}{M_w}^{-0.5}(q'')^{0.67} \qquad \text{Eq. (10)}$$

And E and S are:

$$E = \left(1 + x_e Pr_l \left(\frac{v_g}{v_l} - 1\right)\right)^{0.35} \quad \text{Eq. (11)}$$

$$S = \left(1 + 0.55 E^{0.1} {Re_{lo}}^{0.16}\right)^{-1} \quad \text{Eq. (12)}$$

2.1.1.2.2.2 Condensation

There are less available condensation heat transfer correlations than evaporation ones. Shah film condensation correlation [11] has been chosen here for being an old broadly tested correlation.

$$h_{tp} = h_l \left[(1 - x_e)^{0.8} + \frac{3.8 x^{0.76} (1 - x_e)^{0.04}}{{P_r}^{0.38}}\right] \quad \text{Eq. (13)}$$

Where x is the vapour quality, p_r is reduced pressure $P_r = P/P_{critical}$ and h_l is Dittus-Boelter single phase heat transfer coefficient for the liquid.

2.1.1.3 Pressure drop

Considering the studies that Lee and Mudawar developed in evaporators field [12], total pressure drop in a heat exchanger can be expressed as:

$$\Delta P_{tot} = \Delta P_c + \Delta P_{sp,pre} + (\Delta P_f + \Delta P_a)_{tp} + \Delta P_{sp,sub/super} - \Delta P_e \quad \text{Eq. (14)}$$

Pressure drop inside a heat exchanger where phase change is happening includes the sudden contraction loss at the channels inlet and a sudden expansion recovery at the channels outlet. However, these two terms are not included when calculating pressure drop in this thesis because they are considered to be out of the study. A single-phase pressure drop term is included corresponding to the flow before the phase change conditions are achieved, meaning a vapour pre-cooling in condensers or a liquid pre-heating in evaporators. The two phase pressure drop term consists of frictional and accelerational components. Finally, another single phase flow term is included corresponding to sub-cooling or super-heating that can occur in condensers or evaporators, respectively, when phase change is completed.

2.1.1.3.1 Two-phase pressure drop models

2.1.1.3.1.1 Homogeneous Equilibrium Model (HEM)

The homogenous equilibrium model is based on the assumption that the two-phase mixture behaves as a pseudo-single phase fluid with mean properties weighted relative to vapour and liquid content, and that only latent heat may be exchanged between the phases. Property variations resulting from pressure changes along the channel result in complicated terms that account kinetic energy, flashing and compressibility. The resulting pressure gradient may be expressed as:

$$-\left(\frac{dP}{dz}\right)_{tp} = \frac{\frac{2f_{tp}}{d_h}G^2\left(v_l + x_e v_{lg}\right) + \frac{4q'' G v_{lg}}{d_h\left(h_{lg} + G^2 v_{lg}\left(x_e v_g + (1-x_e)v_l\right)\right)}}{1 + G^2\left(x_e\frac{dv_g}{dP} + (1-x_e)\frac{dv_l}{dP}\right)\left(1 - \frac{G^2 v_{lg}\left(x_e v_g + (1-x_e)v_l\right)}{h_{lg} + G^2 v_{lg}\left(x_e v_g + (1-x_e)v_l\right)}\right) - \left(\frac{G^2 v_{lg}\left(x_e\frac{dH_g}{dP} + (1-x_e)\frac{dH_l}{dP}\right)}{h_{lg} + G^2 v_{lg}\left(x_e v_g + (1-x_e)v_l\right)}\right)} \quad \text{Eq. (15)}$$

The first term in the numerator of Eq. (13) is the frictional gradient and the second the accelerational. The denominator includes kinetic energy, flashing and compressibility terms. The two-phase pressure drop can be determined by integrating Eq. (13) numerically along the stream-wise direction.

$$\Delta P_{tp} = \int_0^{L_{tp}} -\left(\frac{dP}{dz}\right)_{tp} \quad \text{Eq. (16)}$$

The two-phase friction factor f_{tp} is a function of the two-phase Reynolds number Re_{tp}:

$$Re_{tp} = \frac{G d_h}{\mu_{tp}} \quad \text{Eq. (17)}$$

There are several two-phase viscosity models, McAdams [13] proposed the following:

$$\frac{1}{\mu_{tp}} = \frac{x_e}{\mu_g} + \frac{(1-x_e)}{\mu_l} \quad \text{Eq. (18)}$$

2.1.1.3.1.2 Separated Flow Model (SFM)

In separated flow models gas and liquid are considered to flow apart from each other. In these types of models accelerational and frictional terms are treated separately. The first one is expressed in terms of pipe inlet and outlet:

$$\Delta P_a = G^2\left(\left(\frac{v_g x_{e,out}^2}{\alpha_{out}} + \frac{v_l\left(1-x_{e,out}\right)^2}{(1-\alpha_{out})}\right) - \left(\frac{v_g x_{e,in}^2}{\alpha_{in}} + \frac{v_l\left(1-x_{e,in}\right)^2}{(1-\alpha_{in})}\right)\right) \quad \text{Eq. (19)}$$

Where the void fraction is determined from Zivi's [14] relation:

$$\alpha = \left(1 + \left(\frac{1-x_e}{x_e}\right)\left(\frac{v_l}{v_g}\right)^{\frac{2}{3}}\right)^{-1} \quad \text{Eq. (20)}$$

One of the most popular frictional pressure drop correlation is the one proposed by Friedel [15]:

$$\Delta P_f = \frac{2f_{lo}G^2 L_{tp} v_l}{d_h x_{e,out}}\int_{x_{in}}^{x_{out}} \phi_{lo}^2 dx \quad \text{Eq. (21)}$$

$$\phi_{lo}^2 = A_1 + \frac{3.24 A_2 A_3}{Fr_{tp}^{0.045} We_{tp}^{0.035}} \quad \text{Eq. (22)}$$

$$A_1 = (1-x_e)^2 + {x_e}^2 \left(\frac{\rho_l f_{go}}{\rho_g f_{lo}}\right) \quad A_2 = {x_e}^{0.78}(1-x_e)^{0.224} \quad A_3 = \left(\frac{\rho_l}{\rho_g}\right)^{0.91} \left(\frac{\mu_g}{\mu_l}\right)^{0.19} \left(1-\frac{\mu_g}{\mu_l}\right)^{0.7} \quad \text{Eqs. (23,24,25)}$$

$$Fr_{tp} = \frac{G^2}{g d_h \bar{\rho}^2} \qquad We_{tp} = \frac{G^2 d_h}{\bar{\rho}\sigma} \qquad \bar{\rho} = \frac{1}{x_e v_g + (1-x_e) v_l} \quad \text{Eqs. (26,27,28)}$$

It is decided to use HEM pressure drop correlation as the default one. SFM with Friedel correlation may be used to compare results if necessary.

2.1.1.3.2 Single-phase pressure drop model

Following relation is used to determine pressure drop in single phase flow[16, 17]:

$$\Delta P_{sp} = \frac{2 L_{sp}}{d_h} f_{sp} G^2 v \quad \text{Eq. (29)}$$

The single phase friction factor f_{sp} has different values depending on the flow regime. Two linking interpolation functions have been defined to guarantee function continuity.

For $Re \leq 1950$:

$$f_{sp} = f_{lam} = \frac{24}{Re}(1 - 1.3553\beta + 1.9467\beta^2 - 1.7012\beta^3 + 0.9564\beta^4 - 0.2537\beta^5) \quad \text{Eq. (30)}$$

Where β is the channel aspect ratio, which is equal to one for a circular cross section pipe and then:

$$f_{lam} = \frac{14.2296}{Re} \quad \text{Eq. (31)}$$

For $1950 < Re < 2050$

$$f_{sp} = interpolation(f_{lam}(Re), f_{trans}(Re), Re) \quad \text{Eq. (32)}$$

For $2050 \leq Re \leq 19050$:

$$f_{sp} = f_{trans} = 0.079 Re^{-0.25} \quad \text{Eq. (33)}$$

For $19050 < Re < 20050$

$$f_{sp} = interpolation(f_{trans}(Re), f_{tur}(Re), Re) \quad \text{Eq. (34)}$$

For $20050 < Re$

$$f_{sp} = f_{tur} = 0.046 Re^{-0.2} \quad \text{Eq. (35)}$$

2.2 Finite difference methods

In this chapter different basic finite difference methods are explained.

The principle of a finite difference method is that the derivatives in the partial differential equation are approximated to linear combinations of function values at the grid points. So, having a domain and a grid like the following:

$$a < x < b \qquad t > 0$$

$$x_i = a + ih, \quad i = 0, 1, \dots, N, \quad h = \frac{b-a}{N}$$

$$t^k = k\Delta t, \quad k = 0, 1, \dots,$$

The function values for each grid point will be:

$$u_i \approx u(x_i)$$

First order derivative can be defined with any of these three equalities:

$$\frac{\partial u}{\partial x}(\bar{x}) = \lim_{h\to 0}\left(\frac{u(\bar{x}+h) - u(\bar{x})}{h}\right) = \lim_{h\to 0}\left(\frac{u(\bar{x}) - u(\bar{x}-h)}{h}\right)$$

$$= \lim_{h\to 0}\left(\frac{u(\bar{x}+h) - 2u(\bar{x}) - u(\bar{x}-h)}{2h}\right) \qquad \text{Eqs. (36,37,38)}$$

Resulting from that definition, three first derivative approximations can be done:

- The forward finite difference

$$D_+u(\bar{x}) = \frac{u(\bar{x}+h) - u(\bar{x})}{h} = u'(\bar{x}) + \frac{h}{2}u''(\xi) \qquad \text{Eq. (39)}$$

  Therefore the absolute error ξ of the forward finite difference is proportional to h and the approximation is referred as a first order approximation.

- The backward finite difference

$$D_-u(\bar{x}) = \frac{u(\bar{x}) - u(\bar{x}-h)}{h} = u'(\bar{x}) - \frac{h}{2}u''(\xi) \qquad \text{Eq. (40)}$$

  Which is again a first order approximation.

- The central finite difference

$$D_0 u(\bar{x}) = \frac{u(\bar{x}+h) - 2u(\bar{x}) - u(\bar{x}-h)}{2h} = u'(\bar{x}) + \frac{h^2}{6}u'''(\xi) \qquad \text{Eq. (41)}$$

The error ξ is proportional to h^2 so the approximation is referred as a second order approximation. Note that:

$$D_0 u(\bar{x}) = \frac{1}{2}(D_+ u(\bar{x}) + D_- u(\bar{x})) \qquad \text{Eq. (42)}$$

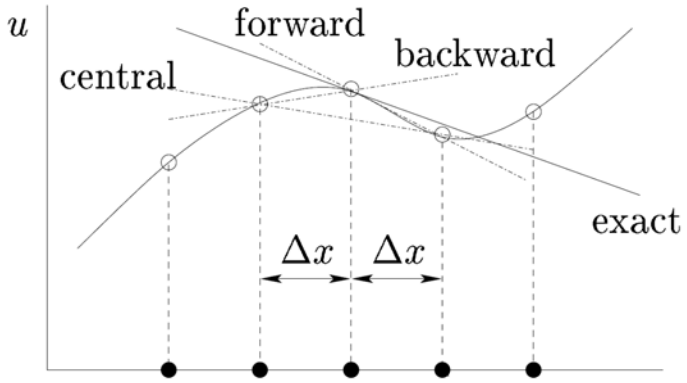

Figure 4 - Geometric interpretation of the different approximations

Approximation to high orders derivatives can be obtained from the formulas for lower order derivatives. The central finite difference scheme for the second order derivative u_{xx} is:

$$D_0^2 u(\bar{x}) = D_+ D_- u(\bar{x}) = D_+ \frac{u(\bar{x}) - u(\bar{x}-h)}{h} = \frac{u(\bar{x}-h) - 2u(\bar{x}) + u(\bar{x}-h)}{h^2}$$
$$= u_{xx}(\bar{x}) + \frac{h^2}{12}u^{(4)}(\xi) \qquad \text{Eq. (43)}$$

So it is a second order approximation.

The one dimension heat equation with a source is an equation of interest in this thesis. It is a parabolic partial differential equation:

$$\frac{\partial u}{\partial t} = \frac{\partial}{\partial x}\left(\beta \frac{\partial u}{\partial x}\right) + f(x,t) \qquad \text{Eq. (44)}$$

If β is a constant value and the partial derivatives are presented in their shorter way, the equation can be written like this:

$$u_t = \beta u_{xx} + f(x,t) \qquad \text{Eq. (45)}$$

The forward Euler method (forward in time, central in space) is:

$$\frac{u_i^{k+1} - u_i^k}{\Delta t} = \beta \frac{u_{i-1}^k - 2u_i^k + u_{i+1}^k}{h^2} + f_i^k \qquad \text{Eq. (46)}$$

$$k = 0, 1, \dots, \qquad i = 1, 2, \dots, N-1,$$

where the boundary conditions $u(a,t)$ and $u(b,t)$ are given,

and where u_i^k is an approximation to $u(x_i, t^k)$ and $f_i^k = f(x_i, t^k)$.

The main characteristic of this scheme is that there is only one unknown value which is the function value in the next time step for this grid point u_i^{k+1}. That means that each new function value in each grid point can be calculated apart from the others.

However, to guarantee stability in a forward scheme the Δt should satisfy the time step restriction:

$$0 < \Delta t < \frac{h^2}{2\beta}$$

This time step restriction can imply a big disadvantage when talking about computational time consuming.

The truncation error of this method is first order in time and second order in space $O(\Delta t + h^2)$.

On the other hand, the same equation written in backward difference scheme (also called implicit scheme) is:

$$\frac{u_i^{k+1} - u_i^k}{\Delta t} = \beta \frac{u_{i-1}^{k+1} - 2u_i^{k+1} + u_{i+1}^{k+1}}{h^2} + f_i^{k+1} \qquad \text{Eq. (47)}$$

In an implicit scheme the only known value is u_i^k so a linear equation system needs to be solved for every new time step.

The truncation error is also $O(\Delta t + h^2)$. The good point of this backward Euler method scheme is unconditionally stable, meaning that Δt could take any value.

Comparison between these methods

The explicit or forward finite difference scheme it is usually easier to implement because it goes one equation by one equation and that makes it simply to develop. However, the time step restriction is a hard disadvantage because it can cause high computational resources consumption.

The implicit or backward finite difference scheme has the really attractive property of being always stable, it does not matter which is the value of time step. That property gives the model a really robust behaviour which is a valuable characteristic when programming. However, this scheme is more difficult to implement because of the matrix system that needs to be created.

3 Calculations

3.1 Case of study

This thesis focuses in a shell and tube multistream LNG heat exchanger. Specifically, only its basic element is going to be studied. A multipass shell and tube MSHE is composed of hundreds of shell tubes while each of them has as tubes inside as streams are left.

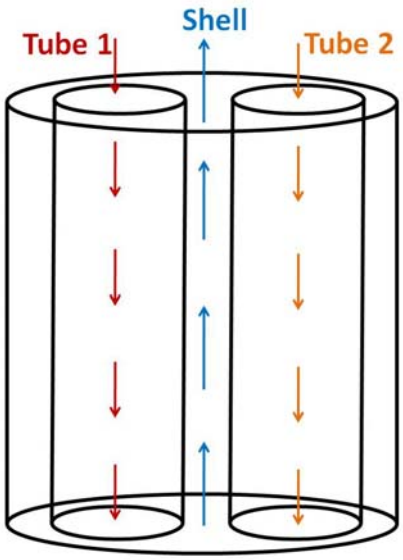

Figure 5 - Shell and two tubes multistream heat exchanger scheme

Since the dynamics of a multistream shell and tubes heat exchanger is a complex phenomenon to model, a simpler case will be studied in this thesis. The dynamics of a counter flow shell and tube heat exchanger have been modelled. In the tube side natural gas is liquefied while in the shell side mixed refrigerant vaporizes. Although it is a simpler case, it has proved to be a considerable challenge.

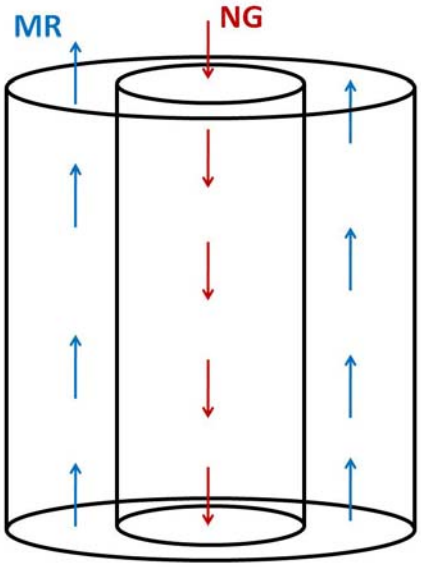

Figure 6 - Shell and tube heat exchanger scheme

Since flow maldistribution is part of the heat exchangers problematic where better designing tools are needed, mass flow in this model is not a fixed value but depends on the difference between the inlet and outlet pressures.

Another important issue that has to be taken into account to achieve better heat exchanger designs is fluid properties dependence on state. In the model, fluid properties are given by TP_library, which is a thermodynamic package created by SINTEF Refrigeration Engineering which returns its user several fluid properties for a certain thermodynamic state.

3.1.1 Counter flow heat exchanger: Natural gas liquefaction

In this case the natural gas phase change from liquid to gas is modelled.

3.1.1.1 General data

The composition of the natural gas used in the model is the following:

Table 1 – Natural gas and mixed refrigerants composition

	Natural gas	Mixed refrigerant
Mole fraction CH_4	0.94480	0.29130
Mole fraction C_2H_6	0.00580	0.38870
Mole fraction C_3H_8	0.01890	0
Mole fraction n-C_4H_{10}	0.00110	0.22710
Mole fraction N_2	0.02950	0.09290
Critical pressure [bar]	56	44.16

Since through TP_library critical pressures are not directly obtainable, natural gas and mixed refrigerant critical pressures have been set at these approximate values. When accurate results are desired, these values should be checked and replaced if necessary.

The geometrical data of the heat exchanger is:

Table 2 – Tube and shell geometrical data

	Tube	Shell
Inner diameter [mm]	4	10
Roughness [µm]	1	1
Length [m]	2	

The tube material is aluminium. Its properties are considered to be constant and are:

Table 3 - Aluminium properties

Density [kg/m^3]	2700
Intensive heat capacitance [J/kgK]	930.77

Aluminium heat conductivity is not displayed because it is assumed to be infinite.

3.1.1.2 Starting conditions

When the simulation begins, the natural gas in the tube side is considered to be in a uniform superheated vapour state at 298K and 49.2 bar. Tube wall temperature at the $t = 0s$ is 297K through all its length. Finally, mixed refrigerant starting conditions are superheated vapour at 296K and 4.7 bar through all the heat exchanger length.

3.1.1.3 Boundary conditions

3.1.1.3.1 Tube side

Natural gas inlet enthalpy is the one corresponding to superheated vapour at 298K and it keeps constant during all the simulation time. Outlet pressure is kept constant at 49.2 bar while inlet pressure raises from 50 at $t = 0s$ till 55 bar at $t = 30s$.

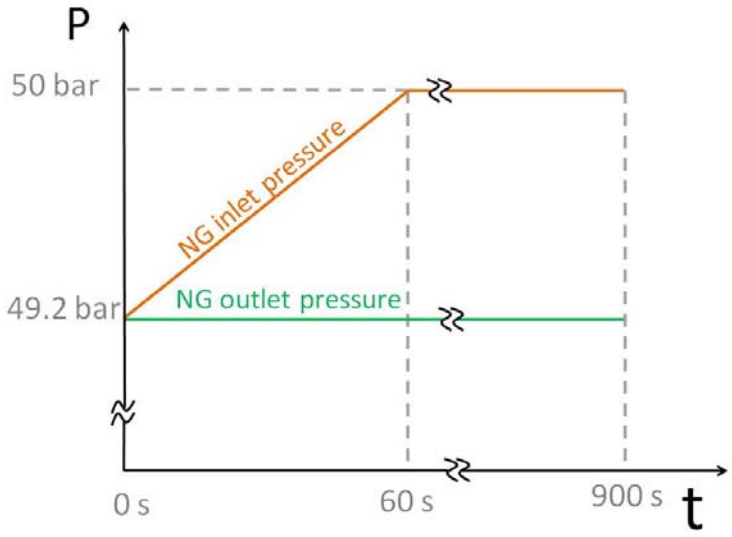

Figure 7 - Natural gas input pressure dependence on time

3.1.1.3.2 Shell side

Mixed refrigerant inlet enthalpy at $t = 0s$ is the one corresponding to superheated vapour at 296K but it decreases till being subcooled liquid at 110K at $t = 60s$.

Once steady state conditions have been reached, mixed refrigerant inlet temperature is raised again to observe the thermal dynamic behaviour of the heat exchanger. Inlet temperature raises from 110K at $t = 500s$ to 250K at $t = 520s$ where is maintained till $t = 540s$ and decreased again to 110K at $t = 560s$.

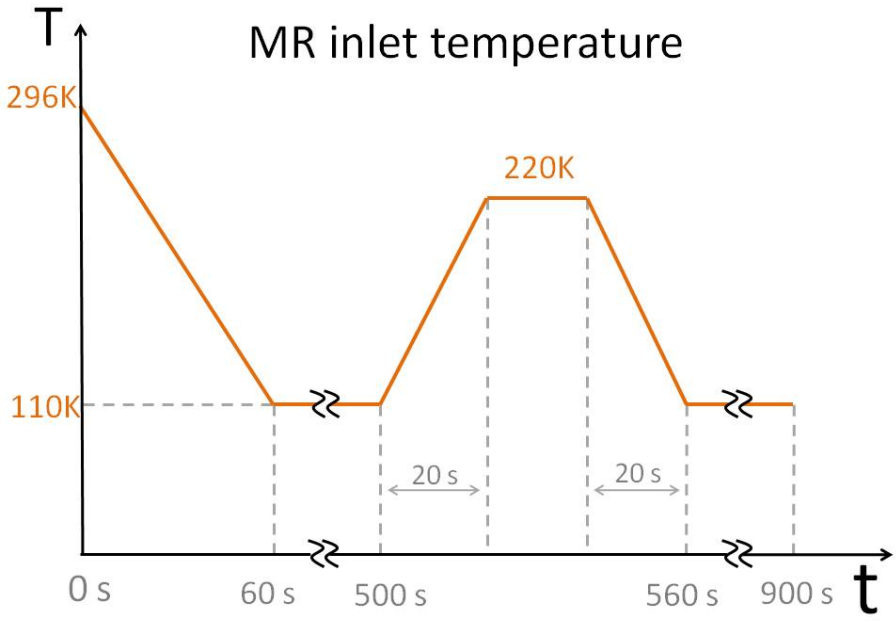

Figure 8 - Mixed refrigerant inlet temperature dependence on time

Inlet and outlet pressures follow an analogous law to natural gas one but with lower values.

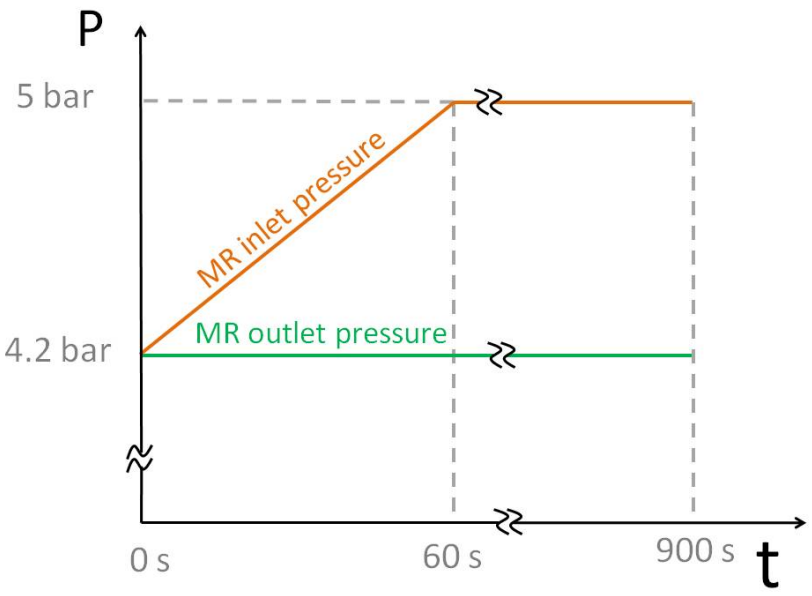

Figure 9 - Mixed refrigerant inlet pressure dependence on time

3.1.1.4 Heat transfer coefficient and pressure drop gradient definition

The correlations selected to be used in the model were described in chapter 6 but the final definition through that makes them continuous through all fluid states has yet to be done. Single phase and two phase correlations need to be linked by some smooth functions, hence, there have to be defined some vapour fractions limits that these functions will link. Here, the lower limit is vapour fraction equal to 0.3 and the upper limit is vapour fraction equal to 0.7.

Equations that define the heat transfer coefficient are the following:

$$\begin{cases} x_e = 0 & h = h_{sp} \\ 0 < x_e < 0.3 & h = f(h_{sp}, h_{tp}) \\ 0.3 \leq x_e \leq 0.7 & h = h_{tp} \\ 0.7 < x_e < 1 & h = f(h_{tp}, h_{sp}) \\ x_e = 1 & h = h_{sp} \end{cases} \quad \text{Eq. (48)}$$

Analogously, equations that define pressure drop gradient are:

$$\begin{cases} x_e = 0 & \Delta P = \Delta P_{sp} \\ 0 < x_e < 0.3 & \Delta P = f(\Delta P_{sp}, \Delta P_{tp}) \\ 0.3 \leq x_e \leq 0.7 & \Delta P = \Delta P_{tp} \\ 0.7 < x_e < 1 & \Delta P = f(\Delta P_{tp}, \Delta P_{sp}) \\ x_e = 1 & \Delta P = \Delta P_{sp} \end{cases} \quad \text{Eq. (49)}$$

3.1.1.5 Simulation accuracy

The grid consists of 40 cells and the convergence criterion is equal to 10^{-3}.

3.2 The model

3.2.1 Procedure

During the period this thesis has been developed, the same procedure has been followed to create and evaluate different models. When developing a model, it has been applied the "from simple to complex" rule, that means that first the whole structure of the model was built without taking into account characteristics that could introduce more instabilities. So first a pipe with fixed and defined wall temperature was modelled where fluid properties, heat transfer coefficient and pressure gradient were considered to be constant. And step by step, more complexity was introduced.

Once the pipe model proved to work correctly with constant fluid properties, real thermodynamics were included by the use of TP_library. So, first the model was checked with pure water, because of the better knowledge of the thermodynamical behaviour of this fluid. Then the model was checked with pure methane as the working fluid which has much more similarities with natural gas but it is still a pure component. Finally, the model was tested with natural gas which as a multicomponent fluid with the effects on its properties that carries represented a higher challenge.

When real fluid properties had been tested satisfactorily in the model, heat transfer and pressure drop correlations were included. First, heat transfer coefficient correlation was included while pressure drop was set constant or following a linear rule with mass flow. Then the opposite situation was followed, pressure drop correlation was included while heat transfer coefficient just followed a simple rule. Finally, both correlations were included.

At the end, once the pipe model had proved to give satisfactory results, the counter flow heat exchanger was modelled following the same calculation structure as in the pipe model.

3.2.2 Structure and operation

The model developed in this thesis allows simulating the dynamics of a counter flow heat exchanger where the two fluids suffer a phase change. In this model the mass flow of a stream is not defined but depends on the difference of the inlet and outlet pressures.

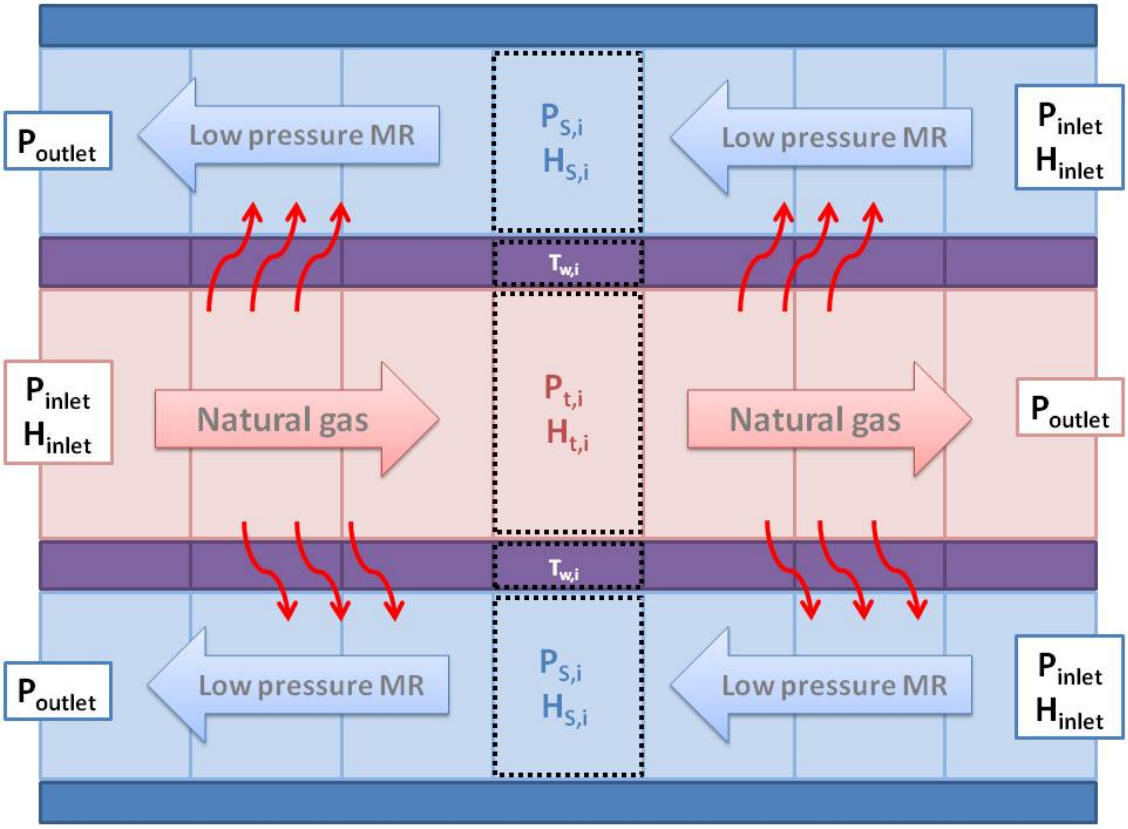

Figure 10 - Discretized scheme of the heat exchanger modelled

The program has been written in MATLAB.

In this model the state of the fluid is set through its enthalpy and pressure. Other variables like temperature and vapour fraction become a consequence of them. The state of the wall is defined by its temperature.

Some assumptions are taken in this model:

- Stable flow.
- Homogenous flow regime.
- Thermodynamic equilibrium.
- Non axial heat conduction.
- Infinite wall thermal conductivity (wall temperature is considered to be the same on both sides of one wall cell).

There are some important characteristics of the final and satisfactory model developed that should be mentioned. First one is that enthalpies and wall temperatures calculations follow

an implicit scheme. The second one is that it presents a varying time step (between established limits) depending on time derivatives. Also, a function that governs the weighting coefficient value in solution relaxation has been implemented. Further explanation of all these is given in this chapter.

The operation of the model follows the scheme below:

1. Mass flow and pressures calculation of both shell and tube streams.
2. Enthalpies calculation of both shell and tube streams.
3. Convergence checking on the streams obtained solutions.
4. Relaxing streams solutions.
5. Other streams variables calculation (temperatures, vapour fractions, heat flows, etc.). A flash call gives the new temperatures and new vapour fractions, then, new heat transfer coefficients and new heat flows can be found.
6. New wall temperatures calculation.
7. Convergence checking on the wall obtained solution.
8. Relaxing wall solution.
9. If both streams and wall convergences were achieved, results are stored and new time step calculations will start. If convergence was not achieved, a new iteration starts again with the recent calculated values.

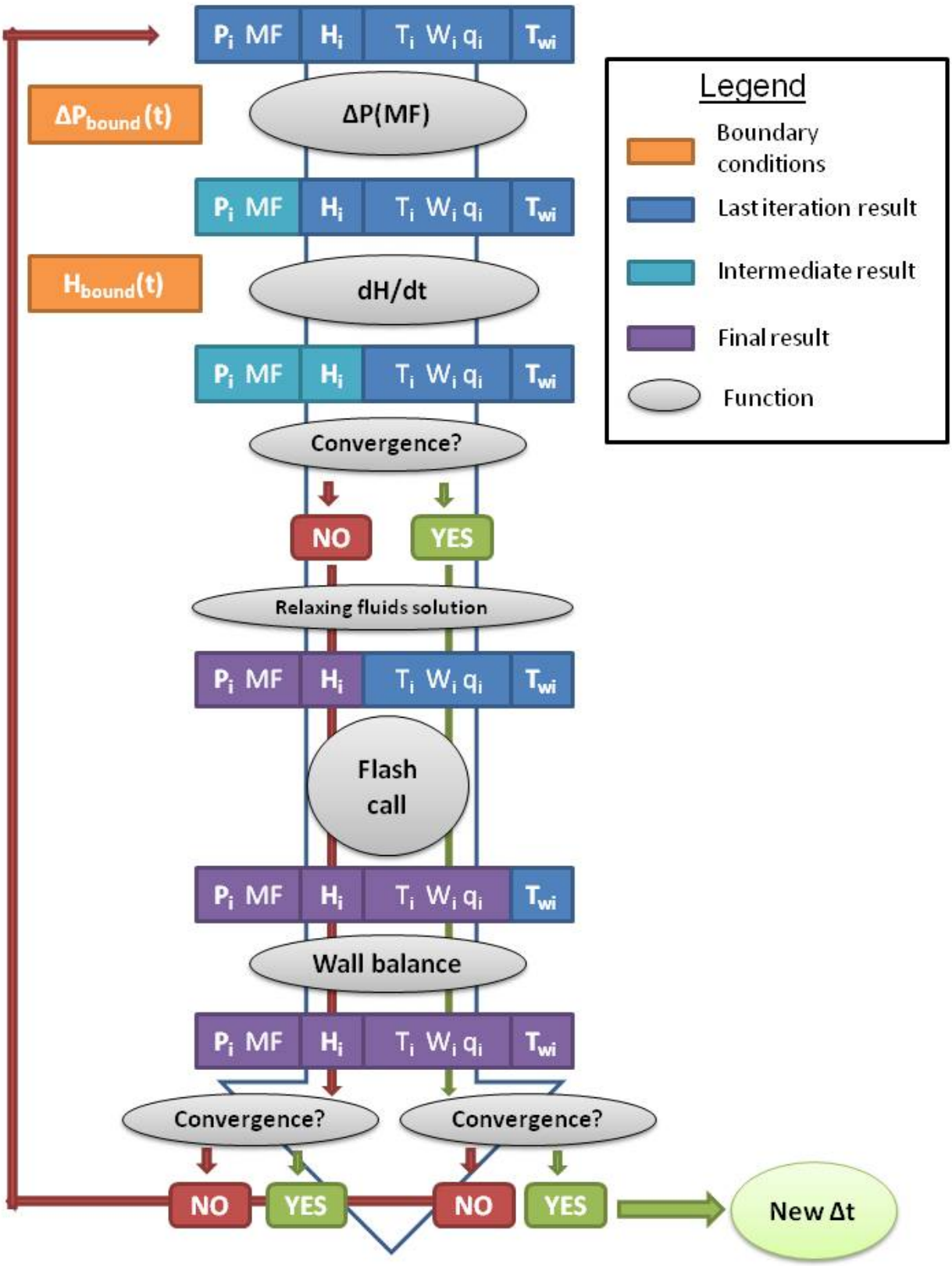

Figure 11 - Model operation scheme

It is asked the reader to note that it is an iterating scheme and that, during calculations between time steps t^k and t^{k+1}, as many iterations as necessary will be done till convergence is reached for all cells.

3.2.2.1 Pressures and mass flow calculation

The total stream pressure drop is the result of the integration of each differential pressure drop along the fluid direction:

$$\Delta P_{Total} = \int_0^L \frac{\partial P}{\partial z} dz \qquad \text{Eq. (50)}$$

When discretized, the total pressure drop becomes a sum of each cell pressure drop. Taking into account that the other variables are kept constant during this calculation, pressure drop depends only on the mass flow.

$$\Delta P_{Total} = \sum_{i=1}^{N} \Delta P_i(\dot{m}) \qquad \text{Eq. (51)}$$

A combination of different numerical methods is used to find the mass flow rate which corresponds to the boundary pressure drop. The secant method, the false position method and the halving intervals method are used here. First, a couple of iterations are done using the secant method to find the upper and the lower limits for the false position method. Then, a certain number of iterations are done with the false position method using its robust but also fast characteristics. If convergence is not achieved after this certain number of iterations, the secant method is used to find the mass flow rate. The halving intervals method is used only when convergence has not been reached by the other two methods.

3.2.2.2 Enthalpies calculation

The following balance equation needs to be solved in the model for each stream:

$$\rho \partial V \frac{\partial H}{\partial t} = \dot{m} \frac{\partial H}{\partial z} + \partial q \qquad \text{Eq. (52)}$$

A scheme of the energy balance for each cell in the tube is the following:

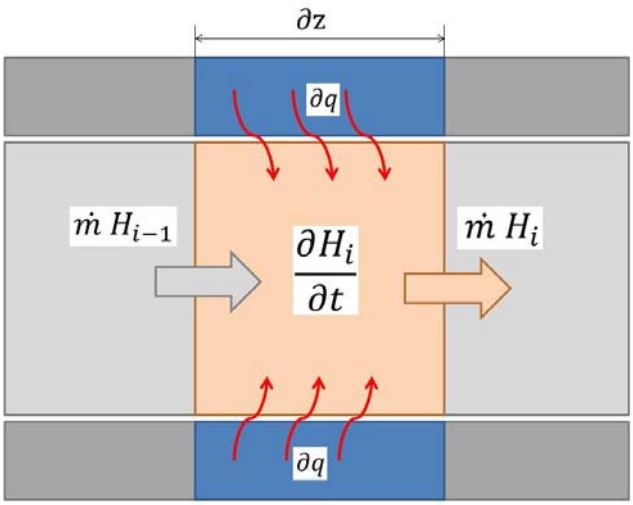

Figure 12 Tube side cell energy balance scheme

When discretized, the implicit scheme form of the Eq.50 is:

$$\rho_i^{k+1} V \frac{H_i^{k+1} - H_i^k}{\Delta t} = \dot{m}^{k+1}(H_{i-1}^{k+1} - H_i^{k+1}) + q_i^{k+1} \qquad \text{Eq. (53)}$$

Where superscripts denote time and subscripts denote position.

However, heat flow depends on several variables (temperature, vapour fraction, ...) that will be found with the flash call, which depend again on the enthalpy. So, heat flows take values from last iteration because is not possible to directly isolate the enthalpy.

As it has been explained in the theory part, an implicit scheme requires solving a system of equations. The linear system that here needs to be solved is:

$$\begin{pmatrix} \frac{\rho V}{\Delta t} + \dot{m} & 0 & \cdots & \cdots & 0 \\ -\dot{m} & \frac{\rho V}{\Delta t} + \dot{m} & \ddots & \vdots & \vdots \\ 0 & \ddots & \ddots & 0 & \vdots \\ \vdots & \vdots & \ddots & \frac{\rho V}{\Delta t} + \dot{m} & 0 \\ 0 & 0 & 0 & -\dot{m} & \frac{\rho V}{\Delta t} + \dot{m} \end{pmatrix} \begin{pmatrix} H_1^{k+1} \\ \vdots \\ H_i^{k+1} \\ \vdots \\ H_N^{k+1} \end{pmatrix} = \begin{pmatrix} \frac{\rho V}{\Delta t} H_1^k + q_1^{k+1} + \dot{m} H_A^{k+1} \\ \frac{\rho V}{\Delta t} H_2^k + q_2^{k+1} \\ \vdots \\ \vdots \\ \frac{\rho V}{\Delta t} H_N^k + q_N^{k+1} \end{pmatrix} \qquad \text{Eq. (54)}$$

MATLAB presents a really powerful characteristics when operating with matrices, so apart from the robust characteristics of the implicit scheme itself, the program gives an extra-advantage in this part of the model.

3.2.2.3 Solution relaxation

Once pressures and enthalpies have been calculated, new states have been found. However, sometimes these results would lead to numerical instabilities. So new states cannot always be the results obtained in the calculation. In some cases it is needed to do a weighting relative between new new-state results and the old new-state results, this is called “relaxing the solution”.

$$y = X \cdot y_{new} + (1 - X) \cdot y_{old} \qquad 0 < X \leq 1 \qquad \text{Eq. (55)}$$

Here y denotes state and is an enthalpy and pressure couple, is the result of an iteration. X is the parameter used to do the weighting. In this model the parameter X is has not a fixed value but depends on the calculation.

When iterating, there are two situations types of situations that could occur. First type is that each iteration gives a new state that it is closer to the real solution than the one before, then it is a stable situation. Second type is that each iteration gives a new state that is further from real solution than the one before. Both types are shown in the following figures:

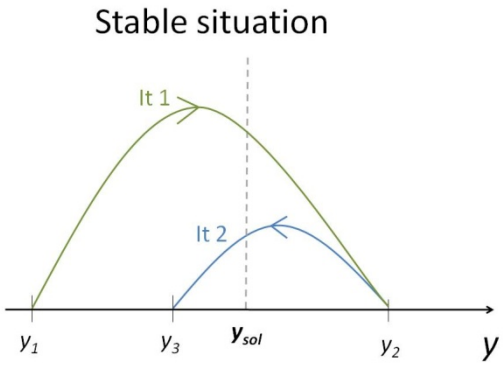

Figure 13 - Numerically stable situation

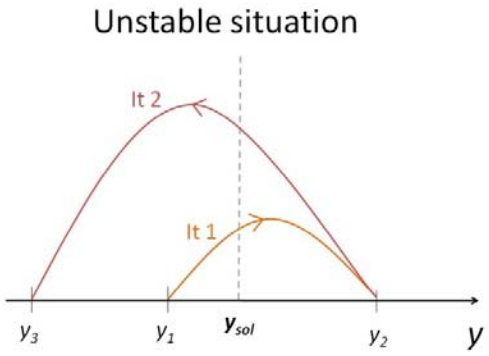

Figure 14 - Numerically unstable situation

The usual strategy when relaxing the solution is to fix the value of the weighting coefficient for all the situations. If the coefficient is low enough and/or the convergence criterion is wide enough, that brings to a stable situation. However, this strategy is not optimal when the situation is stable from the beginning. In a stable situation, a weighting coefficient value lower than one will lead to a higher number of the necessary iterations to achieve convergence than when the value of it is one.

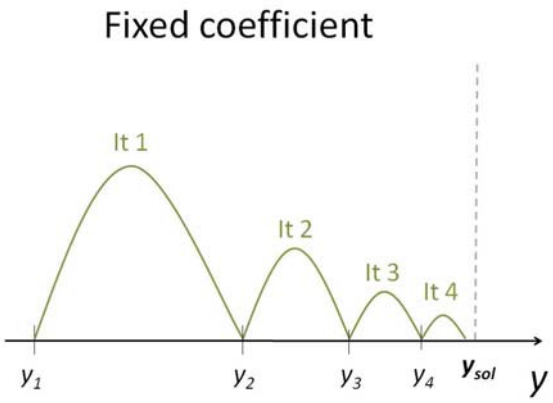

Figure 15 - Fixed coefficient relaxing solution scheme

In the model developed in this thesis the coefficient has not a constant value but changes depending on the results of iteration. Actually, every new time step the coefficient starts having a value equal to X_0. The value of X_0 is set by the user and cannot be higher than 1. In the simulation which results are showed in this thesis, this starting value is:

$$X_0 = 0.5$$

After each iteration, results are checked and the coefficient is decreased or kept constant depending on them. The logical rule that governs the coefficient decreasing is based on the following two characteristics of an unstable situation (see figure 8):

1. Absolute difference between states raises:

$$|y_2 - y_1| < |y_3 - y_2|$$

2. Difference between states changes it sign every iteration:

$$y_2 - y_1 > 0 \qquad y_3 - y_2 < 0$$

If an unstable situation is detected, the weighting coefficient is reduced:

$$X_{new} = 0.95 \cdot X$$

Following that methodology the solution is relaxed only when need, so a fastest and stable solution is achieved:

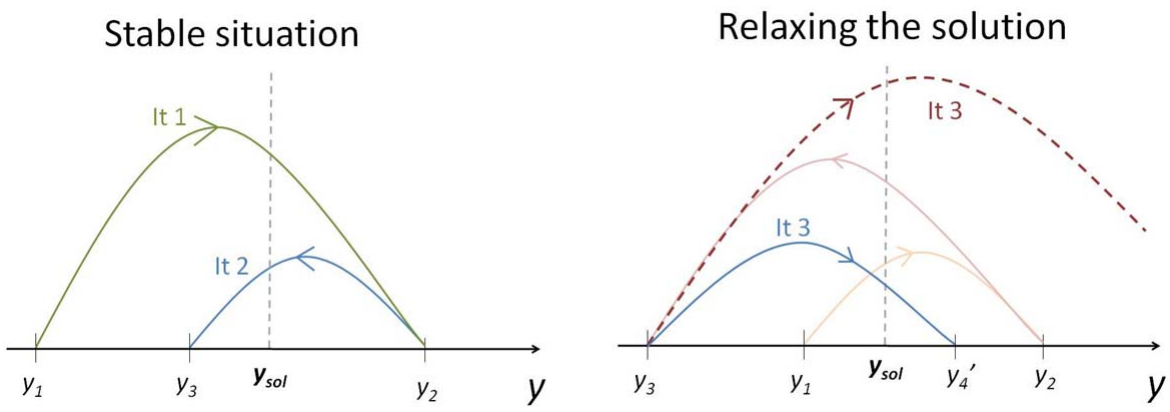

Figure 16 – Behaviour of the relaxing the solution function developed and used in the model

The weighting coefficient has a minimum value that is set by the user.

As it has been explained, fluids states are set by a pressure-enthalpy couple, and there are two streams and several cells for each stream. The relaxing coefficient used in each iteration to calculate new states will have the same value for all cells and in both streams, this means that if one cell is found to be in an unstable situation the relaxing coefficient value will decrease for all of them.

3.2.2.4 Flash call

Once the solution relaxation ends, pressures and enthalpies values have been definitely established, which means that new fluid states have been found. Last step is to find the rest of the variables that are basic for the calculus or may be interesting for the analysis. These variables are: temperature, vapour fraction, heat flow, heat transfer coefficient, etc. Temperature, vapour fraction and liquid and vapour molar compositions are found through the TP_library pressure-enthalpy flash call.

It can numerically happen that enthalpy value is low enough that its related temperature is 0K, if that happens all the fluid properties give false values and the calculus of the model crash. Therefore, a minimum output temperature was set, if the flash output temperature is lower than 60K the cell is considered to be in liquid state at 60K.

Similar situation happens when temperature rises above 1000K, so when that happens the cell is considered to be in vapour state at 1000K.

Apart from flash output variables, heat flow needs to be calculated. The differential form of the heat flow is:

$$\partial q = h\, \partial S_{f,w}\, (T_w - T_f) \qquad \text{Eq. (56)}$$

Here $h = h(H, P, \dots)$ is the convection coefficient, ∂S is the differential fluid-wall contact surface and T_w and T_f are the wall and the fluid temperature.

When discretized:

$$q_i^k = h_i^k S_{cell} \, (T_w^k - T_i^k) \qquad \text{Eq. (57)}$$

The convection coefficient is calculated by an internal function which includes all the necessary correlations which are linked by the pertinent linking functions. An important characteristic that has to be mentioned is that whether a condensing or an evaporating correlation is used in the two phase area depends only on the inlet conditions. If the fluid enters the heat exchanger as liquid, then an evaporating correlation will be used. If the fluid enters the heat exchanger as vapour, then a condensing correlation will be used. That is mentioned because, in a cross flow heat exchanger, heat flow direction could swap locally, which could mean a vapour fraction increasing of a two phase mixture that was expected to condense or, a vapour fraction decreasing of a two phase mixture that was expected to evaporate.

3.2.2.5 Time step function

Time step in the model is not constant, it is changed depending on time derivatives of some of the values of the variables in it. These variables are pressure, enthalpy, mass flow and temperatures. Although the first two are enough to define a state, the other ones have proved to give an accuracy increasing when taking into account. A new time step is set considering that a variable cannot change its value more than a fraction that is set by the user. Then, considering this fraction and the variable time derivative, the maximum time step for each variable is found and the minimum of all is chosen:

$$\Delta t_{P,max} = \frac{\Delta y \cdot P_i^k}{\frac{dP}{dt}}, \quad \Delta t_{H,max} = \frac{\Delta y \cdot H_i^k}{\frac{dH}{dt}}, \quad \Delta t_{T,max} = \frac{\Delta y \cdot T_i^k}{\frac{dT}{dt}}, \quad \Delta t_{\dot{m},max} = \frac{\Delta y \cdot \dot{m}^k}{\frac{d\dot{m}}{dt}}$$

$$\Delta t = \min\left(\Delta t_{P,max}, \, \Delta t_{H,max}, \, \Delta t_{T,max}, \Delta t_{\dot{m},max}\right)$$

Minimum and maximum time step values are set by the user in order to prevent unreasonably short or long time steps.

Since pressure, enthalpy and temperature values depend on the cell, a previous cell maximum time derivative selection has to be done.

Time step is calculated when new time derivatives are not still known, so last values are used to calculate them. However, real new time derivatives may be different than the ones before, so variable changes will be different than predicted.

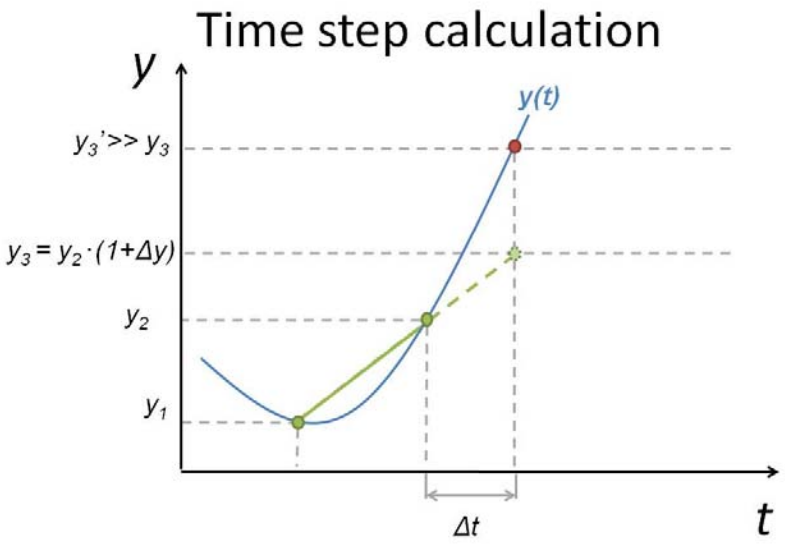

Figure 17 - Model time step function scheme

Although time derivatives can be different than predicted no instabilities will be provoked because of that. In fact, the objective of this function to detailed results during dynamics but allowing fast results when steady state is reached.

3.2.2.6 Linking functions

When heat transfer coefficient and pressure drop correlations are used, a link has to be created between the single phase and the two phase areas in order to guarantee function continuity and, then, numerical stability. It was also observed that just continuity was not always enough to guarantee stability and that its derivative needed to be also continuous. In order to achieve that objective, linking polynomial functions are used in that case. The degree of these polynomials is three and they achieve the continuity of both the function and its derivative.

The first of these two smooth functions link the liquid single phase area with the 0.3 vapour quality two phase area. The second smooth function links the 0.7 vapour quality two phase area with all vapour single phase area. These relatively wide ranges of vapour qualities are needed to achieve the desired characteristics of the functions.

3.2.2.7 Wall energy balance

Considering that it is assumed that wall temperature is equal on both faces of the pipe in the same cell, the energy balance equation that governs the wall temperature is the following:

$$\rho_w \partial V c_{p,w} \frac{dT_w}{dt} = h_{f1} \partial S_{f1,w} (T_{f1} - T_w) + h_{f2} \partial S_{f2,w} (T_{f2} - T_w) \qquad \text{Eq. (58)}$$

Where w denotes wall and $f1$ and $f2$ denote shell and tube fluids respectively.

When Eq.(50) is discretized following the implicit scheme:

$$\rho_w V_{w,cell} c_{p,w} \frac{T_{w,i}^{k+1} - T_{w,i}^{k}}{\Delta t} = h_{f1}^{k+1} S_{f1,w} \left(T_{f1}^{k+1} - T_{w,i}^{k+1}\right) + h_{f2}^{k+1} S_{f2,w} \left(T_{f2}^{k+1} - T_{w,i}^{k+1}\right) \quad \text{Eq. (57)}$$

Wall temperature of time step t^{k+1} can be isolated from Eq.(51):

$$T_{w,i}^{k+1} = \frac{h_{f1}^{k+1} S_{f1,w} T_{f1}^{k+1} + h_{f2}^{k+1} S_{f2,w} T_{f2}^{k+1} + \frac{\rho_w V_{w,cell} c_{p,w}}{\Delta t} T_{w,i}^{k}}{h_{f1}^{k+1} S_{f1,w} + h_{f2}^{k+1} S_{f2,w} + \frac{\rho_w V_{w,cell} c_{p,w}}{\Delta t}} \quad \text{Eq. (59)}$$

4 Results and discussion

4.1 Evaluation of the model robustness and time consumption

The main objective of this thesis was to create a numerically stable model. Therefore, all the functions used in it have been analysed. Linking functions have been created when it has been necessary to avoid discontinuities that could carry numerical instabilities. This study of the numerical behaviour of the model has revealed some facts that are described below.

4.1.1 Phase change at high pressure

Since LNG is produced at high pressures just below its critical point, which in this thesis has been set at 56bar, it was first decided that final inlet and outlet pressures during simulations would be 55 and 54.2 bar respectively. However, these simulations brought always a numerical instability whose origin was finally found and is explained here.

It has been observed that the natural gas phase change at high pressure is a phenomenon where vapour fraction varies abruptly with enthalpy. Besides, it has been noticed that it could be considered a function discontinuity when pressure is high enough. That discontinuity has severe consequences on other functions of the model, like heat transfer coefficient one, and that provokes an irresolvable numerical instability.

The following figures show the vapour fraction and heat transfer coefficient dependence on enthalpy at different pressures. Distance between dots in the phase change is 100 kJ/kg which is a short interval considering the enthalpy magnitude.

Results when pressure is equal to 50bar:

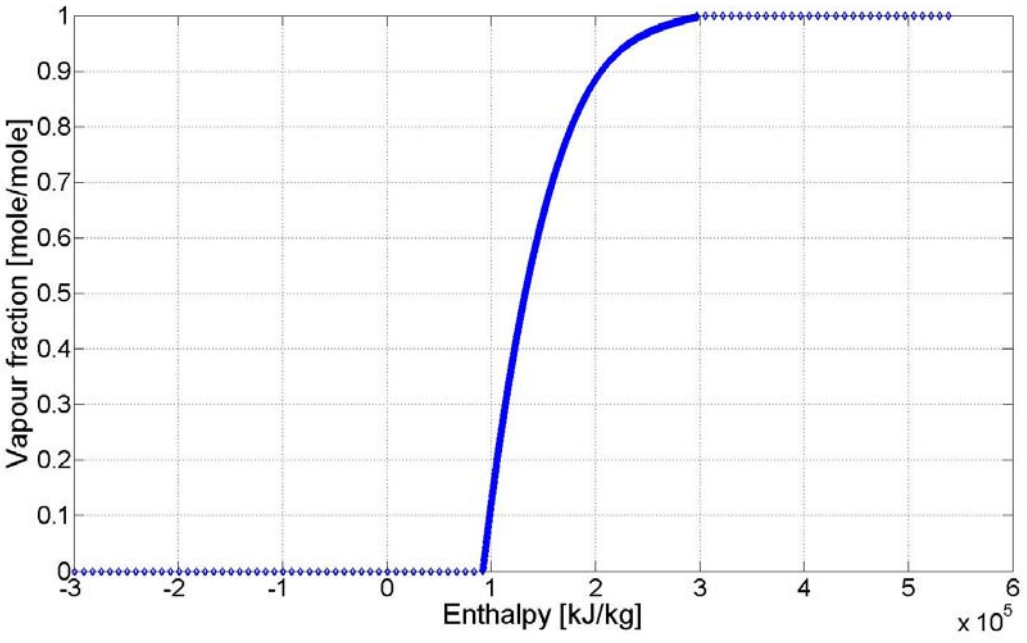

Figure 18 - Vapour fraction vs. Enthalpy at 50bar

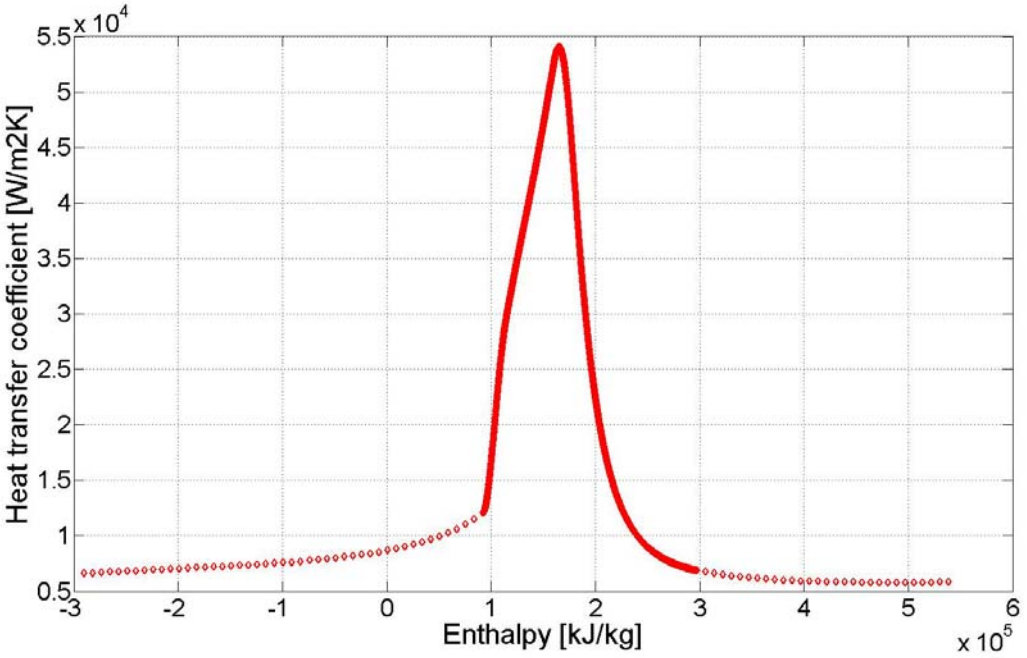

Figure 19 - Heat transfer coefficient dependence vs. Enthalpy at 50bar

Results when pressure is equal to 54bar (here, dots enthalpy interval when $0 < x_e < 0.1$ was set equal to 1 kJ/kg to assure that there was a discontinuity):

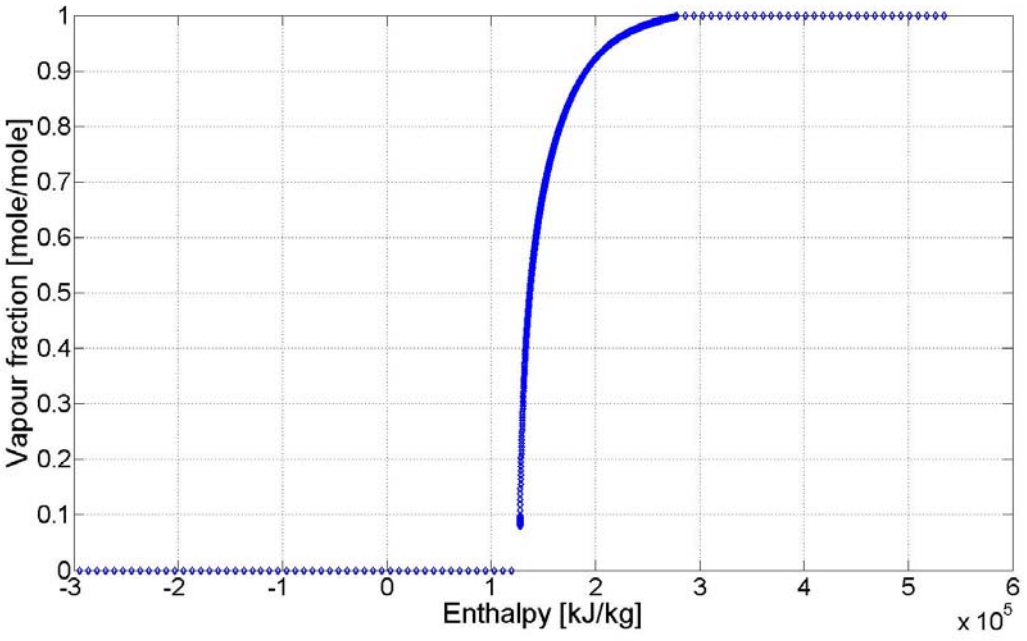

Figure 20 - Vapour fraction vs. Enthalpy at 54bar

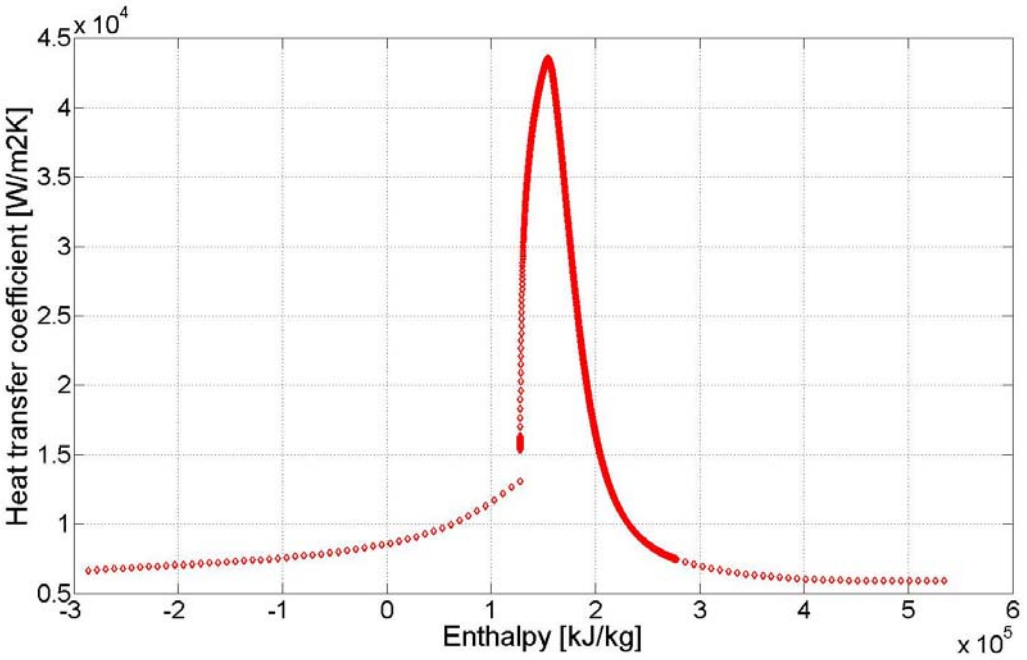

Figure 21 - Heat transfer coefficient vs. Enthalpy at 54bar

Results when pressure is equal to 55bar (here, dots enthalpy interval when $0 < x_e < 0.6$ was set equal to 1 kJ/kg to assure that there was a discontinuity):

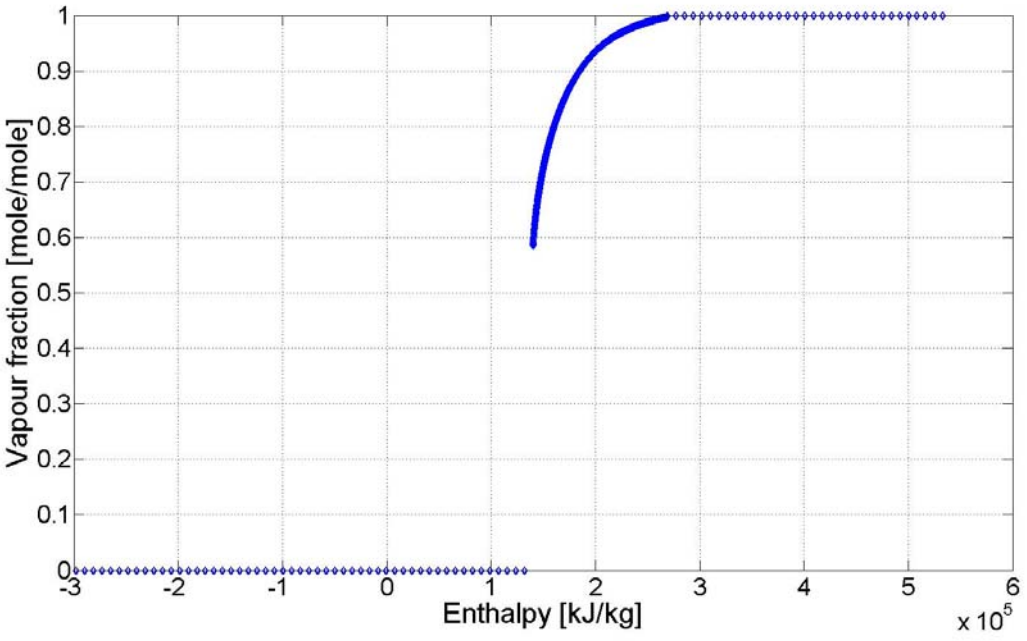

Figure 22 - Vapour fraction vs. Enthalpy at 55bar

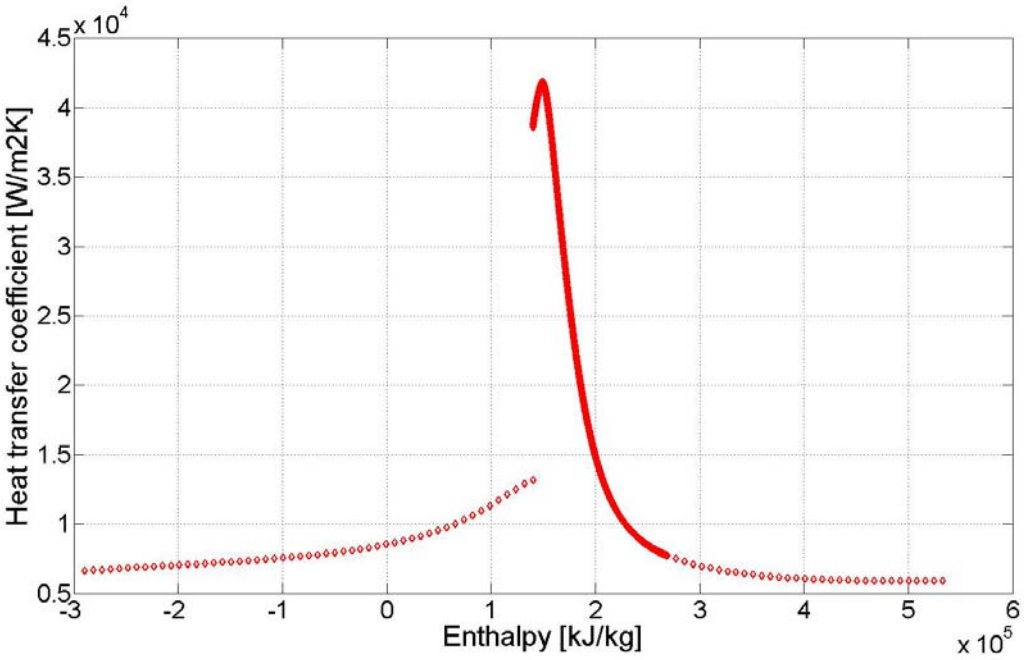

Figure 23 - Heat transfer coefficient vs. Enthalpy at 55bar

Notice that at 54bar it already appears a discontinuity at low vapour fractions. However, at 55bar this discontinuity goes from $x_e = 0$ to $x_e = 0.58$, and that provokes that heat transfer suffers also a discontinuity that goes almost from its minimum value to its highest value, which would be a focus of enormous numerical instabilities.

Since vapour fraction correspondence with enthalpy depends on the flash call, and this one depends itself on the TP_library, there is no possibility of avoiding this vapour fraction discontinuity without losing all the advantages and flexibility that TP_library allows. Therefore, it is decided to reduce the final inlet pressure to 50 bar, which is also a high pressure where in phase change variables present abruptly variations but is continuous.

4.1.2 Gnielinski and Dittus and Boelter heat transfer correlations numerical effects

Another relevant observation that has been noticed during simulations is that correlation election can have an important impact on the numerical oscillations created during calculations, hence, on CPU time consumption.

Two simulations were run to compare Gnielinski and Dittus and Boelter heat transfer correlations numerical effects. All the parameters are the same as described in chapter 8 except from some accuracy parameters that have reduced to increase simulation speed. These changes are:

- Grid: The cells number has been reduced to 20.
- Convergence criterion is set at 10^{-3}.
- Time step function: $\Delta t_{min} = 1s$.

So, once these modifications were done, both simulations were run until $t = 40s$. The following figures show the number of iterations necessary to solve each time step for each simulation:

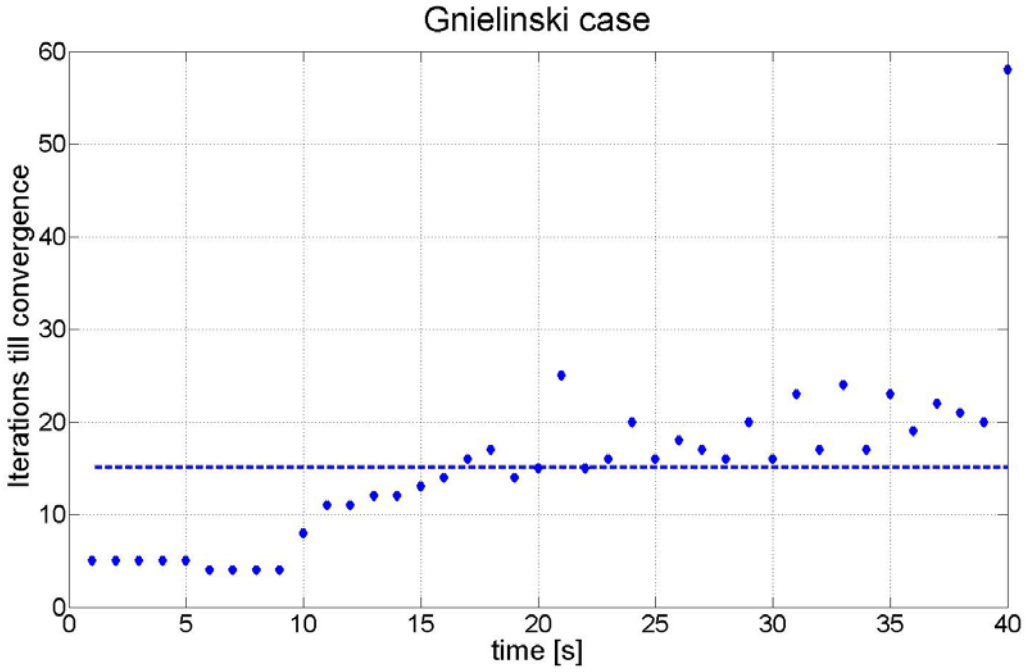

Figure 24 - Number of iterations necessary to achieve convergence when Gnielinski correlation is used

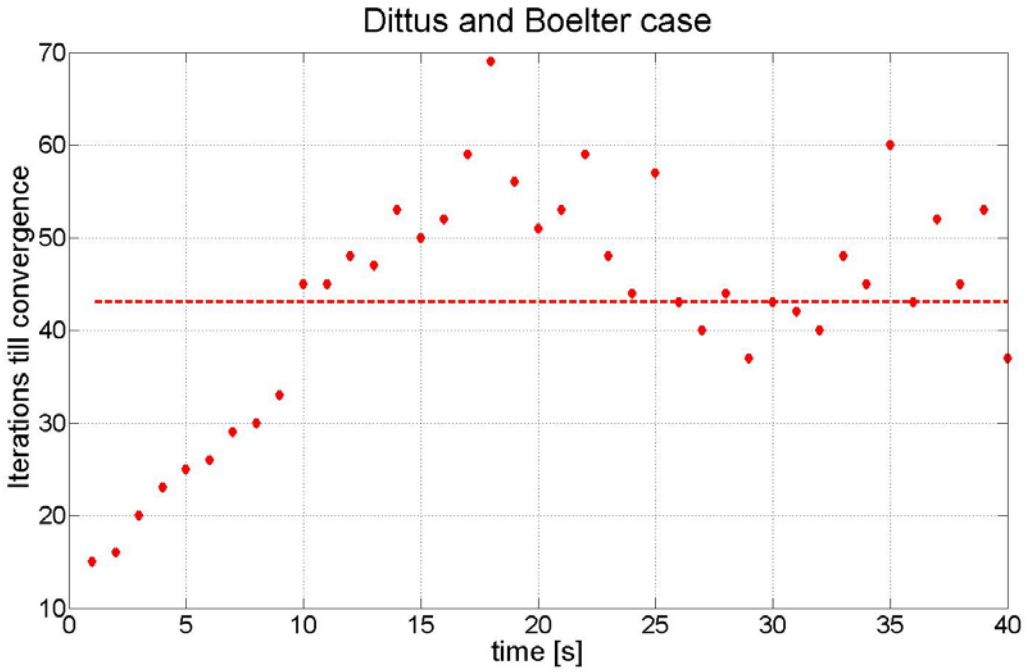

Figure 25 - Number of iterations necessary to achieve convergence when Dittus and Boelter correlation is used

The mean number of iterations used in the simulation where Gnielinski correlation has been used is 15,175 iterations per simulated second, while in the one where Dittus and Boelter

has been used is 43,125. Both correlations would be valid to use in the model but Gnielinski correlation proved to give a faster solution, so this is the correlation used in the model.

4.1.3 Advantages of the varying relaxing coefficient

Since a function was developed just to control the relaxing coefficient value, it was necessary to prove its usefulness.

Same simulation parameters as the ones used to compare correlations were used in a simulation with a fixed relaxing coefficient value (and using Gnielinski correlation).

The relaxing coefficient was fixed at 0.2 and the number of iterations necessary to reach convergence each time is showed in the following plot:

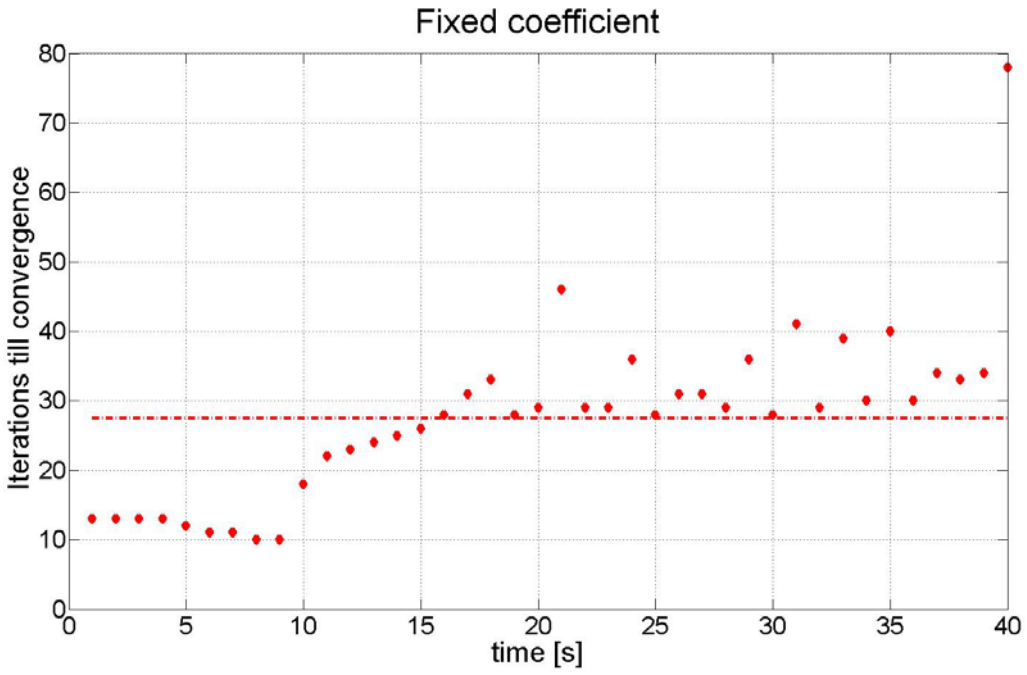

Figure 26 - Number of iterations necessary to achieve convergence when a fixed relaxing coefficient value is used

The mean number of iterations when the coefficient is constant is 27,6 iterations per simulated second, while when it varies is only 15,125 (as showed in figure 24). So, the function developed to control the value of this coefficient proves to give a faster solution.

4.1.4 Effect of time step length and grid meshing on the numerical stability

In linear numerical implicit scheme where parameters in it have a constant value like ones explained in chapter 7, time step length does not jeopardize numerical stability. As explained in chapter 7, only the explicit scheme is under a time step length restriction to avoid instabilities.

However, the model developed in this thesis is a follows a non-linear implicit scheme. Lots of parameters vary with the state (like fluid properties). As a consequence, it has been observed that time step length does compromise the numerical stability of the model. As an

example, same simulation as the one here simulated with a minimum time step of 5s instead of 2s and it conducted to a numerical instability that meant the failure of the simulation.

Similar consequence has been observed when talking about grid meshing. Same simulation run with 20 cells as grid number, instead of 30, produced a severe numerical instability.

It is reasonable to think that big cells under big changes will produce more oscillations, and sometimes instabilities, than smaller cells under smaller changes.

4.2 Case results

This chapter show the obtained results when simulating the case presented in chapter 3.1.

Case of study boundary conditions were set in order to study the behaviour of the heat exchanger during start up conditions and during an abrupt change in the inlet mixed refrigerant temperature.

It is reminded that during the start up, both mixed refrigerant and natural gas inlet pressures increase till $t = 60s$, and from then on are kept at a constant value. Natural gas inlet temperature is kept constant at 298K during all simulation time. However, mixed refrigerant inlet temperature follows law depending on time that is showed in the figure below:

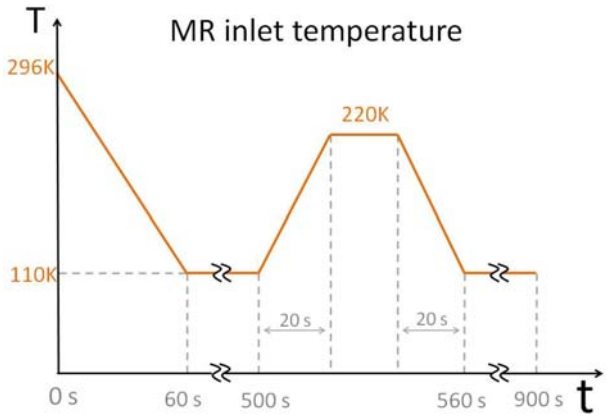

Figure 27 - Mixed refrigerant inlet temperature dependence on time

When the results of a stream are shown for several cells, a code of colours is used to know the position of these cells. This code is the one represented in the next figure:

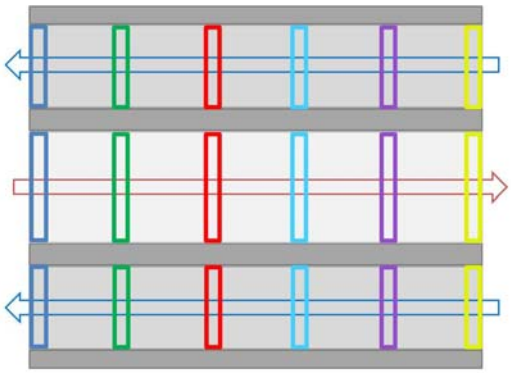

Figure 28 - Code of colours used when plotting different cells of a same stream

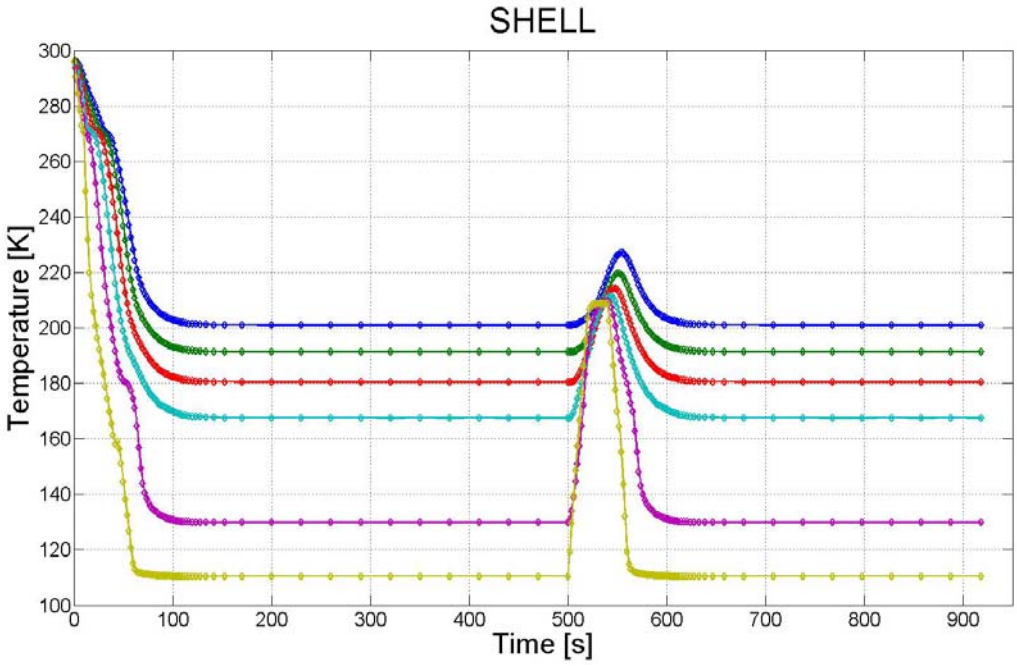

Figure 29 - Mixed refrigerant temperature in several shell cells

Figure above shows the temperatures during the simulated time of several cells in the shell side. Some interesting issues can be explained from it.

First of all, it shows how the start up conditions last till after $t = 100s$ although mixed refrigerant inlet temperature was kept constant from $t = 60s$. So, the system needs approximately 40s to achieve steady state conditions.

Figure 29 also shows the effects of the abrupt change in the mixed refrigerant inlet temperature (see figure 27). Note that MR inlet temperature is kept constant during 20s at 220K but the heat exchanger still responds to it as if it was a peak input.

Focusing on the numeric behaviour on the model, an important characteristic that figure 30 illustrates is the good response of the time step function. Note that time step length decreases when the system is working in transient conditions and as a result detailed information is obtained from the model. Besides, it can also be observed that time step length increases when steady state conditions are reached and that means less CPU time consumption.

Since the system reaches steady state conditions at $t = 100s$, from then on the time step length is 30s. That could have provoked the lost of much of the information about the abrupt change consequences that occurs at $t = 500s$. To avoid this, the model is forced to, first, reach exactly $t = 500s$ and then, in the next calculation use the time step with minimum length. This way of solving this problematic is called “event handling” and some programs like ordinary equations solvers in MATLAB use the same procedure.

Natural gas mass flow rate during the simulated time is shown in the following figure:

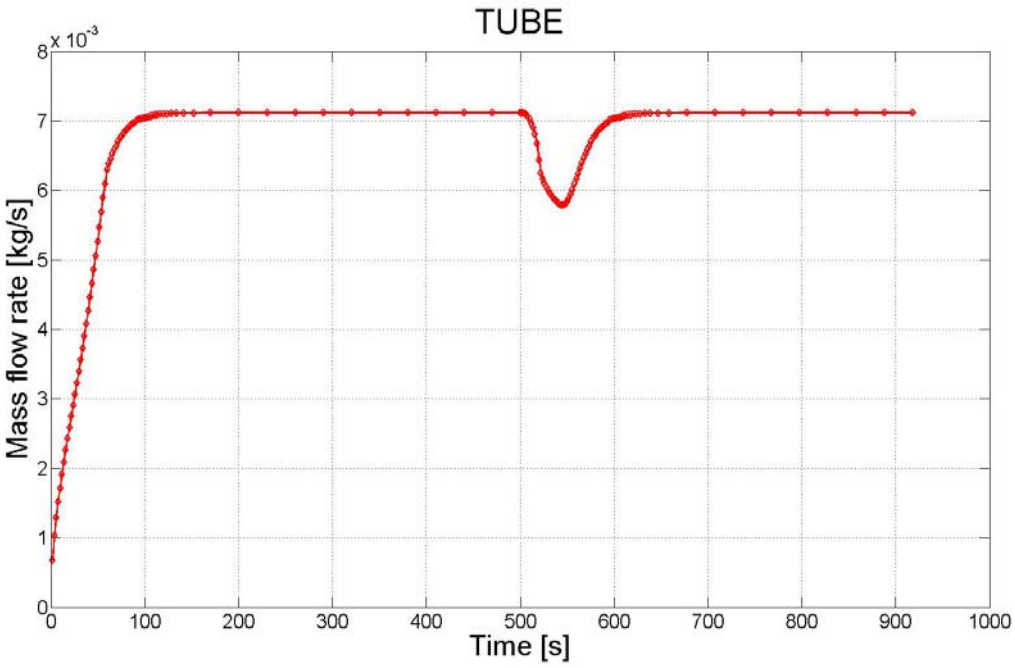

Figure 30 - Natural gas mass flow rate during time

In figure 30 it can be observed again the dynamic behaviour of the system, here, NG mass flow rate during the simulated time. It is interesting to focus in the decrease that the mass flow rate suffers when the MR inlet temperature changes increases abruptly. The cause of that phenomenon is that natural gas outlet phase changes from liquid to vapour. When the cold stream increases its temperature more and more natural gas in vapour state emerges from the tube outlet, considering that pressure drop is constant from $t = 60s$, this increase in the vapour fraction provokes a reduction in the mass flow rate.

MR mass flow rate decreases as a consequence of the same phenomenon. MR inlet vapour fraction increases with the inlet temperature. Consequently, mass flow rate is reduced with inlet temperature increasing.

4.2.1 Thermal dynamics during the start up

One of the most appreciated qualities of this model will be its capability of simulating starts up and shut downs. Therefore, detailed thermal results of the start up in this simulation are given below.

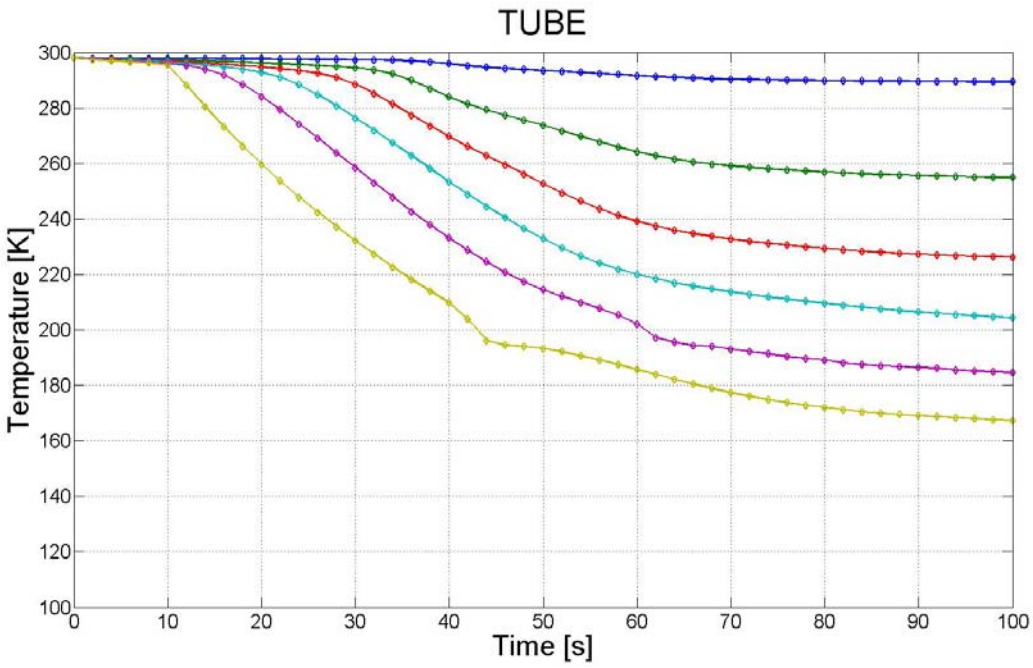

Figure 31 - Natural gas cells temperatures during t<150s

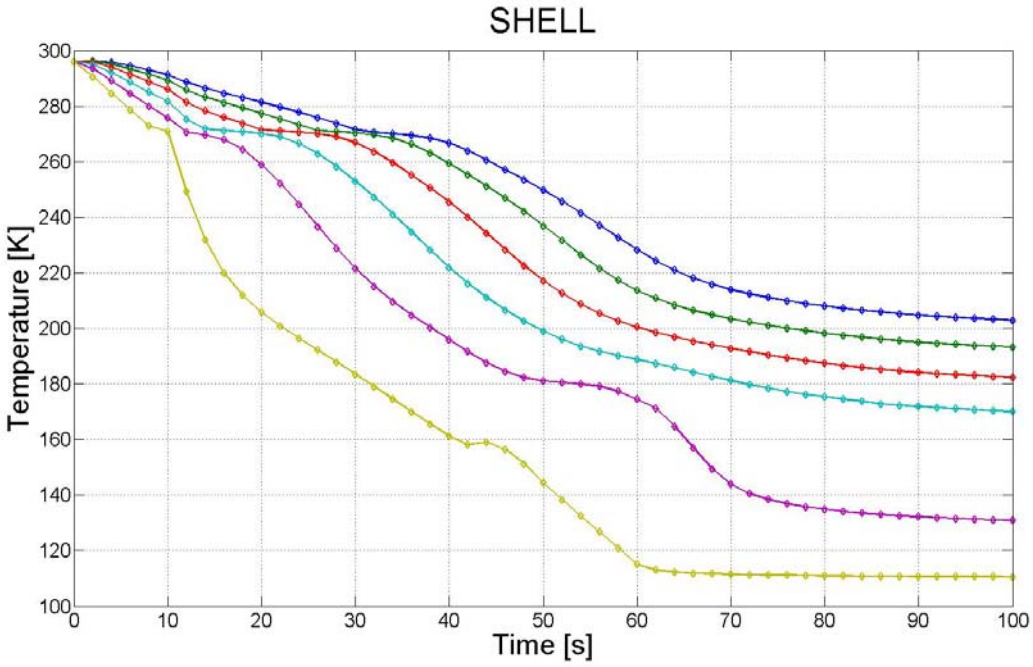

Figure 32 – Mixed refrigerant cells temperatures during t<150s

Upper figures show some cells temperatures of each stream during the start up. It can be seen how MR inlet cell reaches 110K just after $t = 60s$ and is kept constant at that value from then on. However, the rest of the system be considered to be in steady state till $t = 100s$. Some interesting frames of what happens during this period are displayed below:

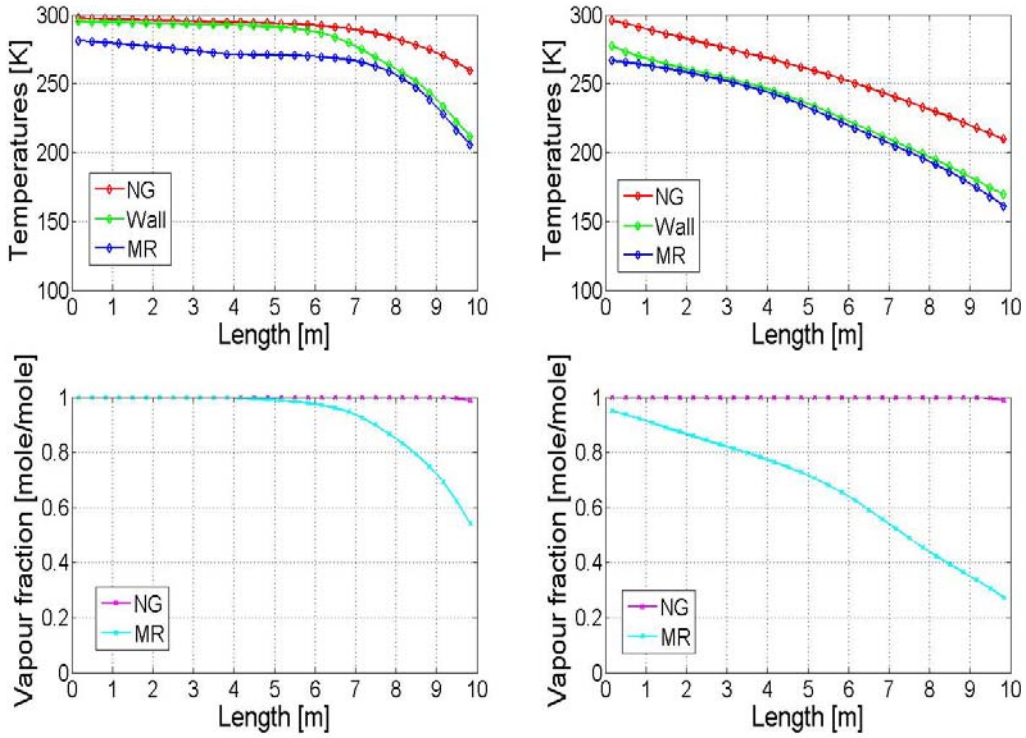

Figure 33 - Temperatures and vapours fractions at t=20s and at t=40s

Figure 33 shows NG, wall and MR temperatures along the length of the heat exchanger in two different time steps, at $t = 20s$ and at $t = 40s$. It also shows vapour fraction of each stream at the specified time steps.

Figure 33 clearly illustrates the influence of the phase change in the wall temperature. It is reminded that NG, wall and MR starting temperature were 298K, 297K and 296K, respectively, so, both streams starting conditions were superheated vapour. However, both frames show that wall temperature reduces considerably its difference with MR temperature when two phase MR flows through the shell side. The cause of that is the increasing of the heat transfer coefficient value; a two heat transfer coefficient value is much higher than the single phase one.

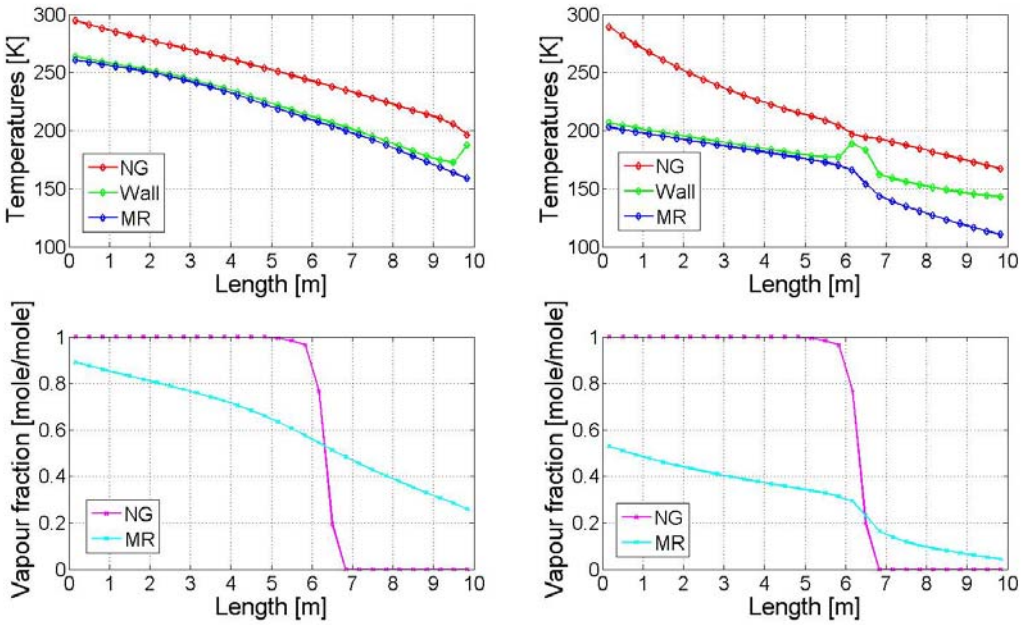

Figure 34 - Temperatures and vapours fractions at t=44s and at t=100s

Figure 34 shows again two frames of the start up. These ones belong to the system state at $t = 44s$ and at $t = 100s$ (steady state).

First feature that has to be highlighted is the rapid NG phase change. As it has been explained in chapter 7.1, NG phase change at high pressures is a abrupt phenomenon. Here, it can be noticed how it became all liquid in just 4s (comparing with figure 33 at $t = 40s$).

Second feature that should be commented about the first frame is that this liquid NG achieves higher heat transfer values and that tights the wall temperature to higher values. This effect is illustrated in the rising of the last cells temperature.

Third and last important displayed characteristic that should be discussed refers to the steady state conditions at $t = 100s$. It can be observed that wall temperature is only closer to NG temperature where the phase change occurs. In the previous meters wall temperature is almost the same as MR temperature. After the phase change, wall temperature drops again to a middle value within both streams temperatures. This feature is, again, consequence of the heat transfer coefficient value depending phase area.

More detailed frames about the start up are displayed in the appendix.

4.2.2 Thermal dynamics during an abrupt change in the shell inlet temperature

These second results show the thermal dynamic behaviour of the heat exchanger model when just one inlet parameter is modified.

As explained in chapter 6.1 and displayed in figure 27, shell inlet temperature suffers a rapid change between 500s and 560s. This change in the inlet conditions has an effect in the whole heat exchanger that is interesting to study.

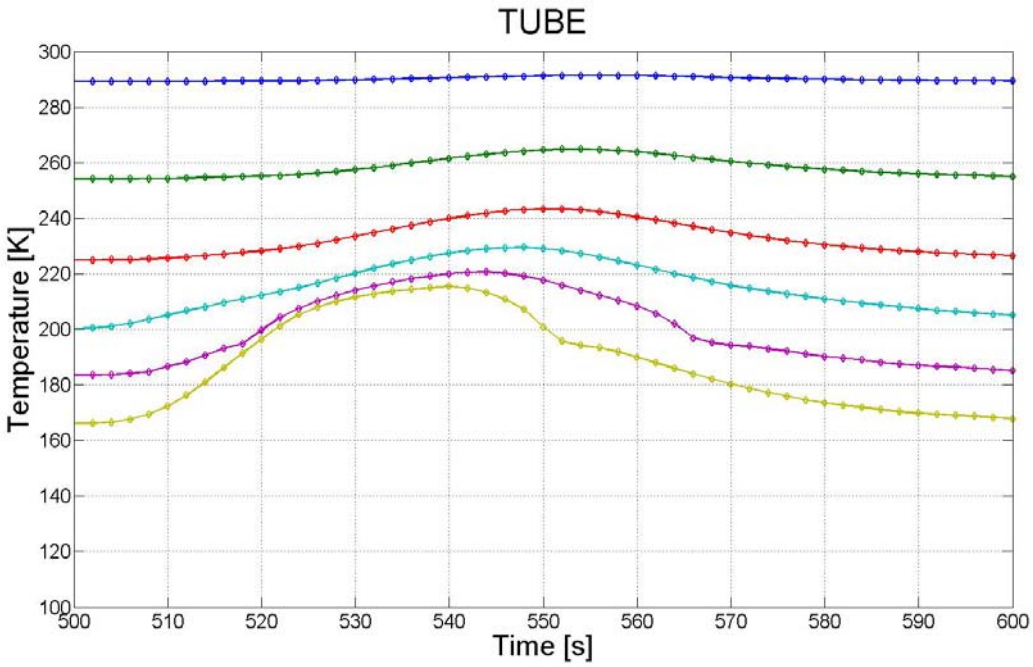

Figure 35 - Natural gas cells temperatures during 500s < t < 600s

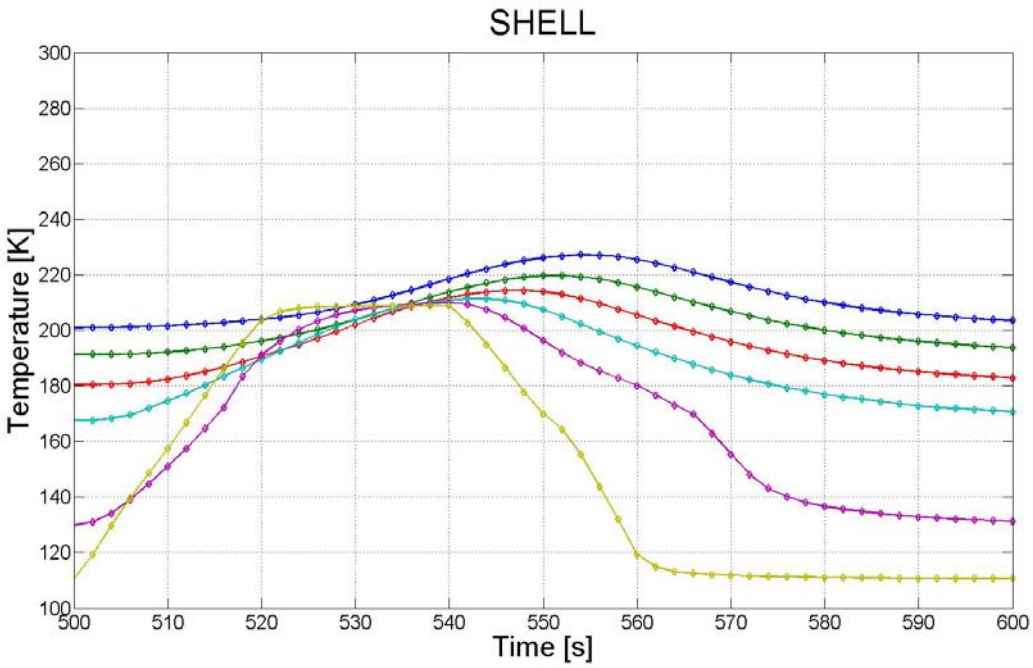

Figure 36 - Mixed refrigerant cells temperatures during 500s < t < 600s

Figures above show some of NG and MR cells temperatures during this period. Notice that although MR inlet temperature keeps constant during 20s at 220K, only MR inlet cell

achieves a stable state during this time while the rest of the system is in constantly change during it.

Figure 35 shows how the effects of this abruptly change are rapidly damped in the tube side.

Notice that, since the model takes into account the fluid movement, there is a delay between the increasing of the MR inlet and outlet temperatures.

An interesting figure that shows the consequences of taking into account this fluid movement is displayed below:

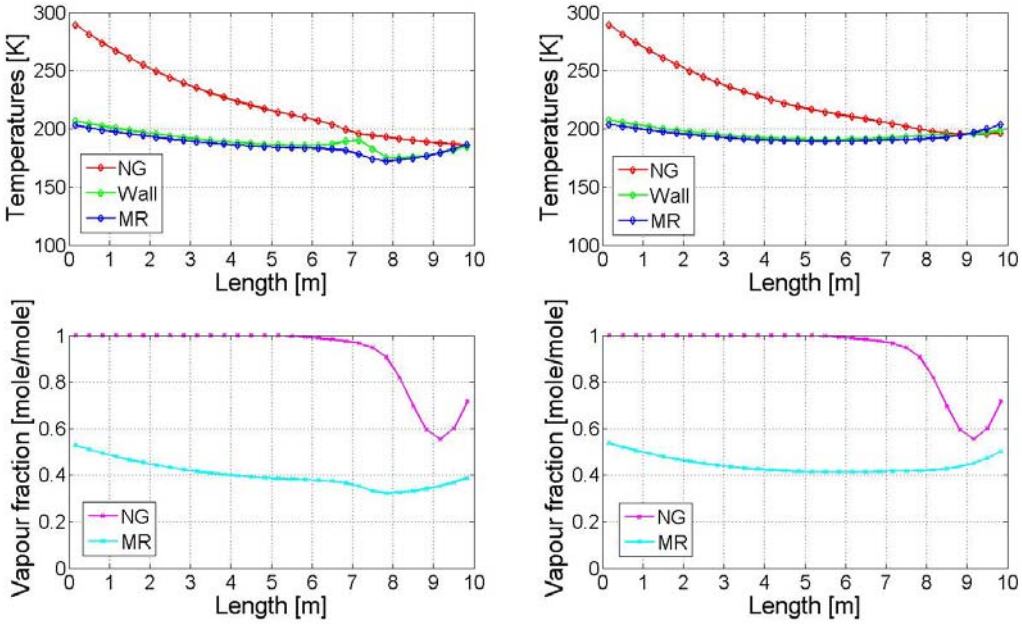

Figure 37 - NG, wall and MR temperatures and NG and MR vapour fractions at t=516s and at t=520s. Cross temperatures phenomenon can be observed at t=520s frame

Figure 37 shows stream and wall states at $t = 516s$ and at $t = 520s$. The already explained effects of the phase change on the temperatures can be observed again. However, since the model takes into account fluid movement, some interesting features can be extracted of them. First, it can be seen in both frames that there is a minimum at $z = 9m$ in the vapour fraction that can only be noticed because fluid movement effect is not neglected.

Notice that at $t = 520s$ MR temperature at shell inlet rises above NG and wall temperatures. That means that there cold and warm streams swapped locally. That is a consequence of taking into account the fluid movement. Since it is a counter flow heat exchanger, NG is facing MR outlet temperature at its inlet and that provokes that NG outlet temperature can be lower than MR temperature when MR inlet temperature is increased rapidly enough.

However, the model does not take into account this cold and warm streams swapping when calculating heat transfer coefficient value. This means that MR two phase heat transfer value

when it is locally warmer is still calculated through an evaporation correlation, which is not correct. However, it has to be considered that changing heat transfer coefficient correlation following heat flow direction would provoke a discontinuity in the heat transfer function that would trigger a severe instability.

More frames about walls and streams states during this period are displayed in the appendix.

5 Conclusions and recommendations for further work

5.1 Conclusions

During the development of this thesis some interesting numerical behaviours related to heat exchanger where phase change occurs have been observed. It has been proved that if the pressure at which the phase change takes place is high enough, it can create a discontinuity in the vapour fraction dependence on enthalpy. This discontinuity affects severely the numeric behaviour of the model, it provokes discontinuities on other functions like heat transfer coefficient one, and that obviously leads to a numerical instability.

A second observation noticed when simulating in this thesis is the importance of the correlations selection. Whether one or other correlation is chosen has an impact on CPU time consumption. For the same input simulation parameters, it has been proved that Dittus and Boelter single phase heat transfer correlation leads to a higher number of necessary iterations to achieve convergence than Gnielinski's.

Another relevant output of this thesis is the development of a simple function that varies the weighting coefficient value when relaxing the solution. This function has been tested against a coefficient with a fixed value and it has proved to produce a faster solution.

It has also been noticed that time step length and cell size have an impact on the numerical instability of the model.

It has been shown that the model results provide detailed information of the heat exchanger dynamics. Time step control can be an appreciated feature of the model. Also, accounting fluid movement has shown some interesting results that would have been skipped if it had been neglected.

The objective of this thesis was to find out if it is possible to develop a numerically stable multistream heat exchanger model where thermal dynamics could be simulated and studied. Pursuing an answer to this objective a stable counterflow heat exchanger model has been satisfactorily developed. This model aims to be a suitable base to continue in the design of the MSHE model.

5.2 Recommendations for further work

Recommendations for further work can be classified into the three following goals:

1. Optimisation of the numerical part of the model.
2. Research of the suitable heat transfer and pressure correlations.
3. Introduction of the developed tool into practical use.

The model developed in this thesis has still to overcome some numerical challenges till presenting the suitable characteristics to be used as a heat exchanger design tool. Stability of the simulations must be guaranteed, hence, further study on the time step length and grid meshing should be considered. It is the writer opinion that improved relaxing solution and time step functions could give much more robustness to the model. Besides, the improvement of these functions could also mean a reduction in the CPU time consumption, which is the numerical challenge that should be faced once stability is guaranteed.

Further research should be done in the correlations field. Finding the correlations that better correspond to the experimental results has not been the goal of this thesis. Therefore, an evaluation of the different available correlations and its accuracy should be carried out. However, it also has to be taken into account the numeric consequences that this correlation may bring. It is reminded that it has been shown in this thesis that correlation selection has an effect on the model numerical response.

Finally, once these and future challenges have been conquered, the model should be used for the real design of a heat exchanger. Model flexibility during the design process and the accuracy of the results may be the main appreciated features.

6 Bibliography

1. Adrian J. Finn, G.L.J., Terry R. Tomlinson, *LNG technology for Offshore and mid-scale plants.* 2000.
2. Julio Cesar Pacío, C.A.D., *A review on heat exchanger thermal hydraulic models for cryogenic applications.* 2011.
3. Fredheim AO, H.R., *Possibilities of cost reductions in base-load.* EUROGAS96. Proceedings from the European applied research conference on natural gas, 1996: p. 101-14.
4. Kanoglu M, D.I., Rosen MA, *Performance analysis of gas liquefaction cycles.* Int. J. Energy Res, 2008.
5. RF, B., *Cryogenic technology.* Ullman's encyclopedia of industrial chemistry. Wiley-VCH Verlag GmbH and Co, KGaA, 2000.
6. Warren M. Rohsenow, J.P.H., Young I. Cho, ed. *Handbook of heat transfer*. 1998.
7. F. W. Dittus, B., *Heat transfer in turbulent pipe and channel flow.* 1930.
8. Gnielinski, V., *New equations for heat transfer in turbulent pipe and channel flow.* Int. Chem. Eng, 1976: p. 359-368.
9. Stefan S. Bertsch, E.A.G., Suresh V. Garimella, *A composite heat transfer correlation for saturated flow boiling in small channels.* Int. J. Heat Mass Transfer, 2009. **52**: p. 2110-2118.
10. Z. Liu, W., *A general correlation for saturated and subcooled flow boiling in tubes and annuli, based on a nucleate pool boiling equation.* 1991.
11. Shah, M.M., *A general correlation for heat transfer during film condensation inside pipes.* 1978.
12. Issam Mudawar, J.L., *Two-phase flow in high-heat-flux micro-channel heat sink for refrigeration cooling applications: Part I pressure drop characteristics.* 2004.
13. W. Qu, I.M., *Measurement and prediction of pressure drop in two phase micro-channels heat sinks.* Int. J. Heat Mass Transfer, 2003. **46**: p. 2737-2753.
14. Zivi, S.M., *Estimation of steady-state void-fraction by means of the principle of minimum entropy production.* ASME J. Heat Transfer 1964. **86**: p. 247-252.
15. J.G. Collier, J.R.T., *Convective boiling and condensation.* third ed., Oxford University Press, 1994.
16. F. P. Incropera, D.P.D., *Fundamentals of Heat and Mass Transfer, fifth ed.* 2002.
17. R. K. Shah, A.L.L., *Laminar Flow Forced Convection in Ducts: A Source Book of Compact Heat Exchanger Analytical Data.* 1978.

7 Appendix

Detailed result frames during simulation's start up period:

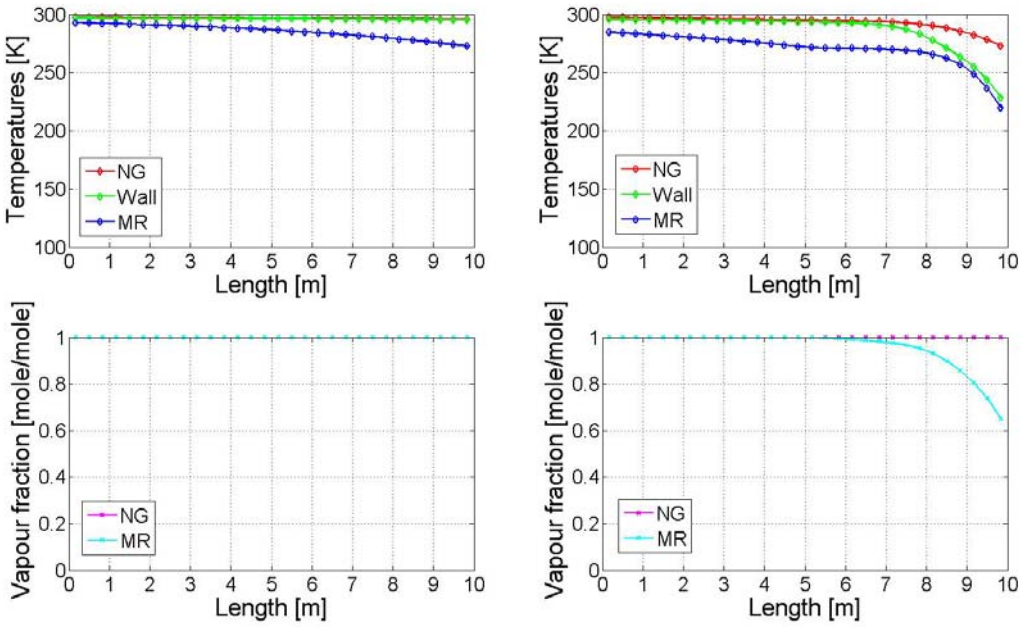

Temperatures and vapour fractions at t=8s and at t=16s

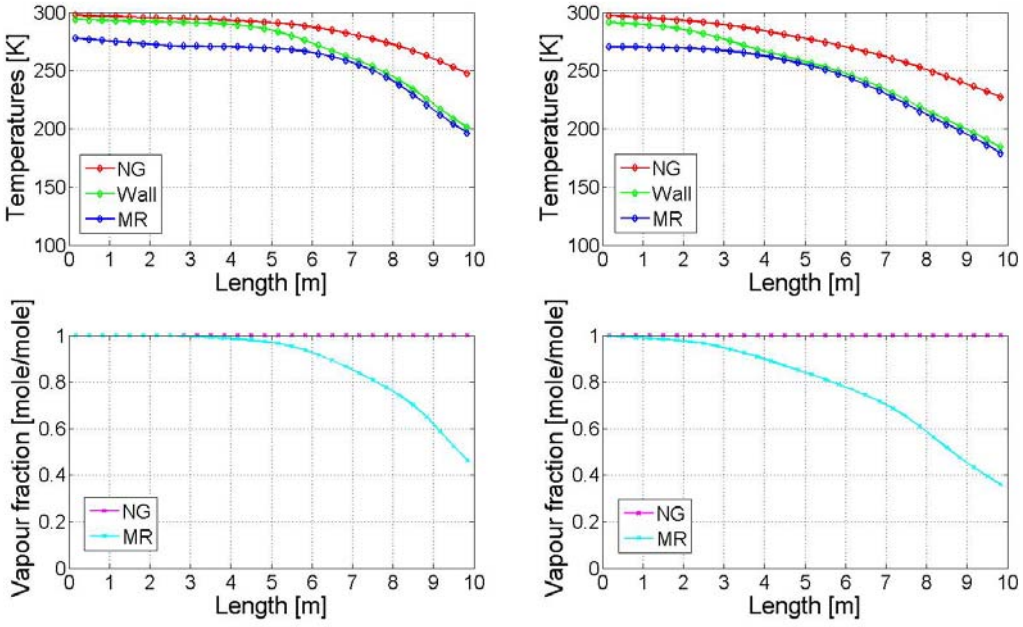

Temperatures and vapour fractions at t=8s and at t=16s

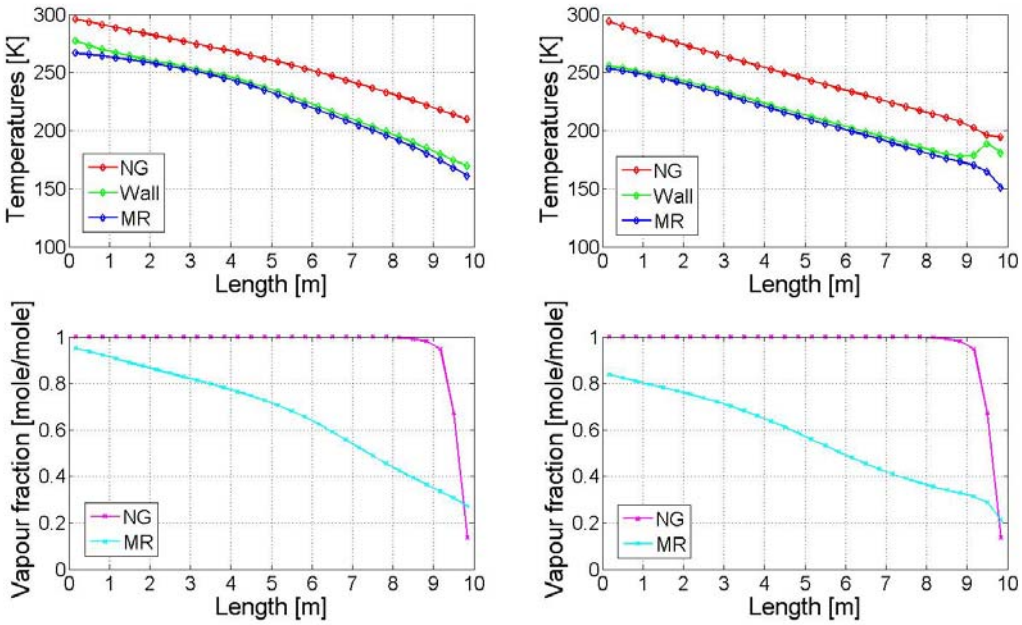

Temperatures and vapour fractions at t=40s and at t=48s

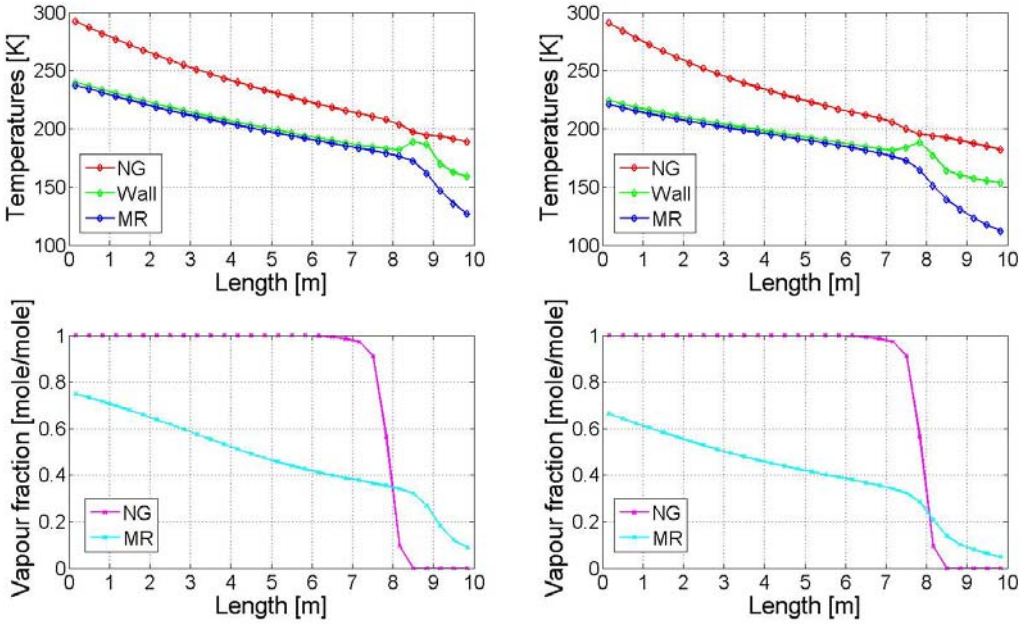

Temperatures and vapour fractions at t=56s and at t=64s

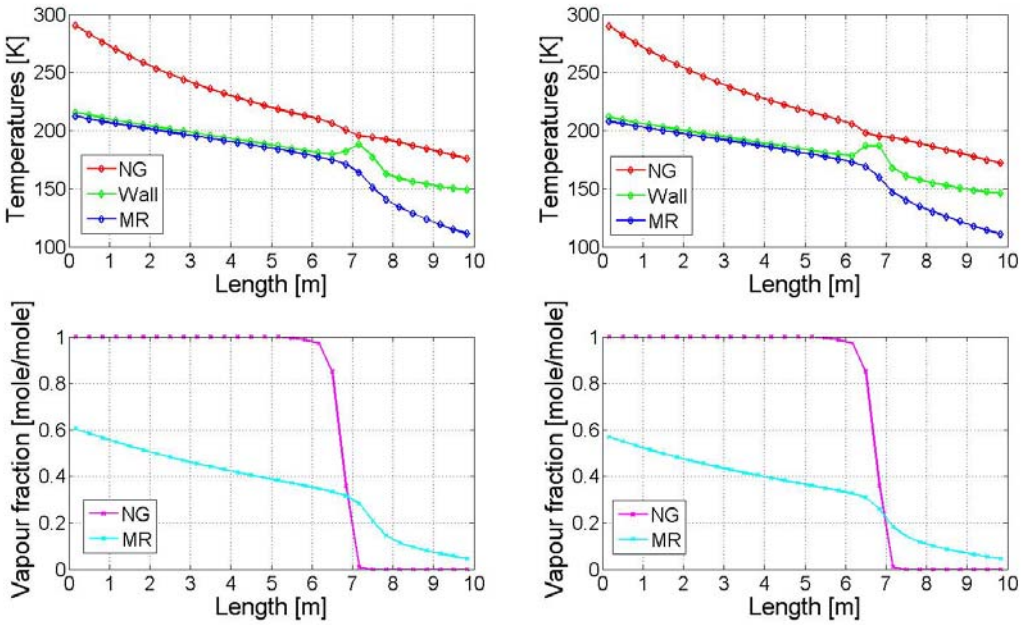

Temperatures and vapour fractions at t=72s and at t=80s

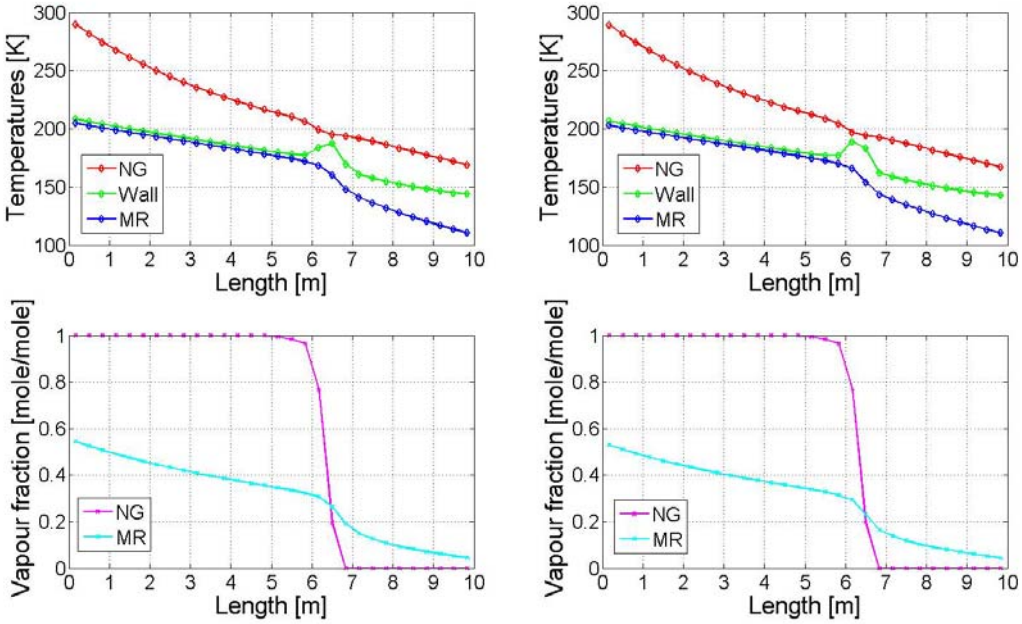

Temperatures and vapour fractions at t=90s and at t=100s

Some frames during the abrupt change of the MR inlet temperature are:

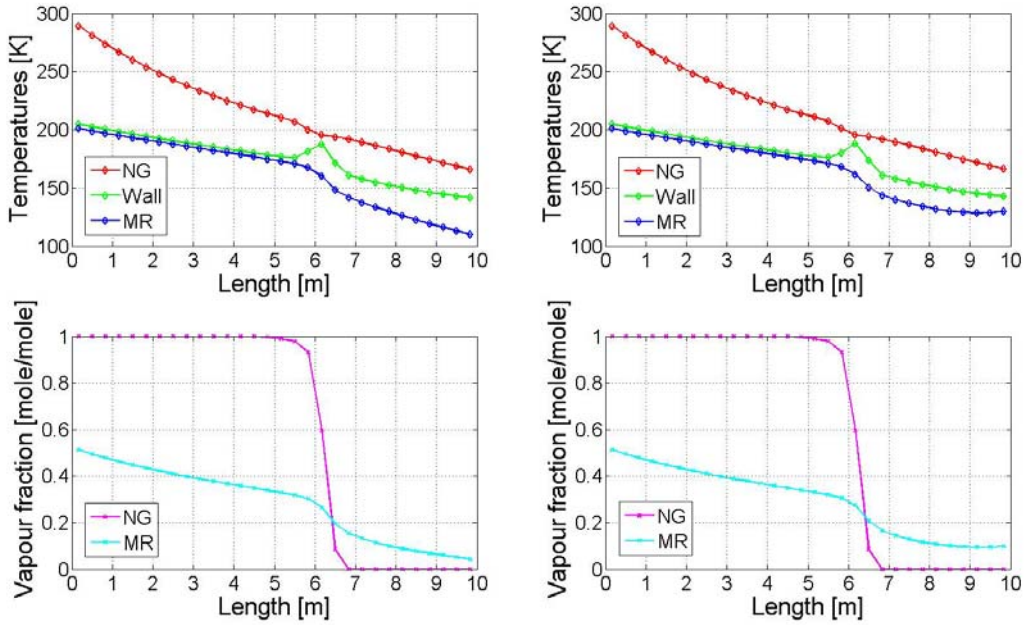

Temperatures and vapour fractions at t=500s and at t=504s

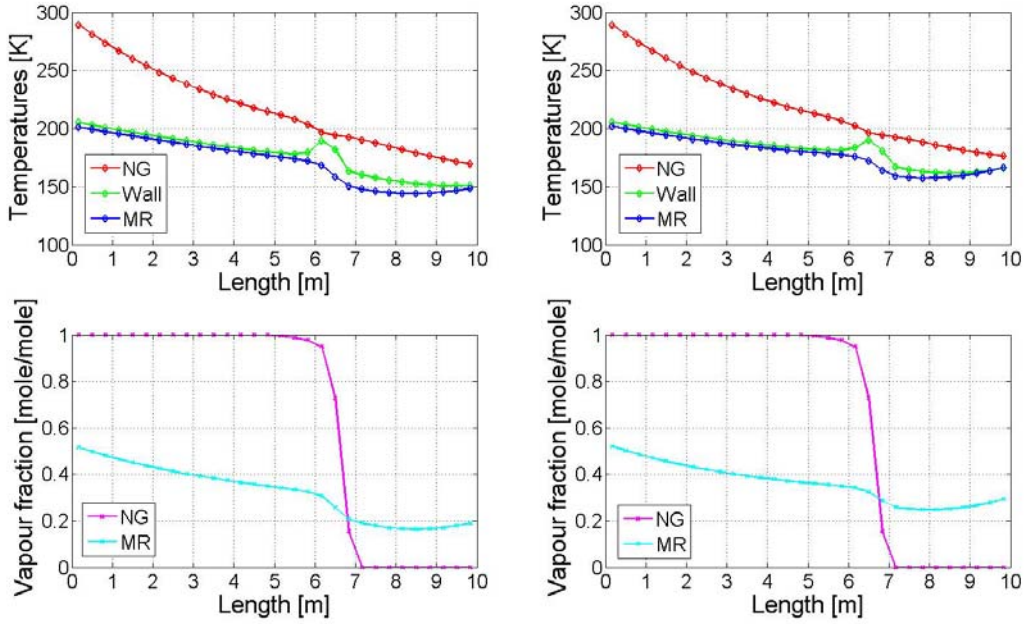

Temperatures and vapour fractions at t=508s and at t=512s

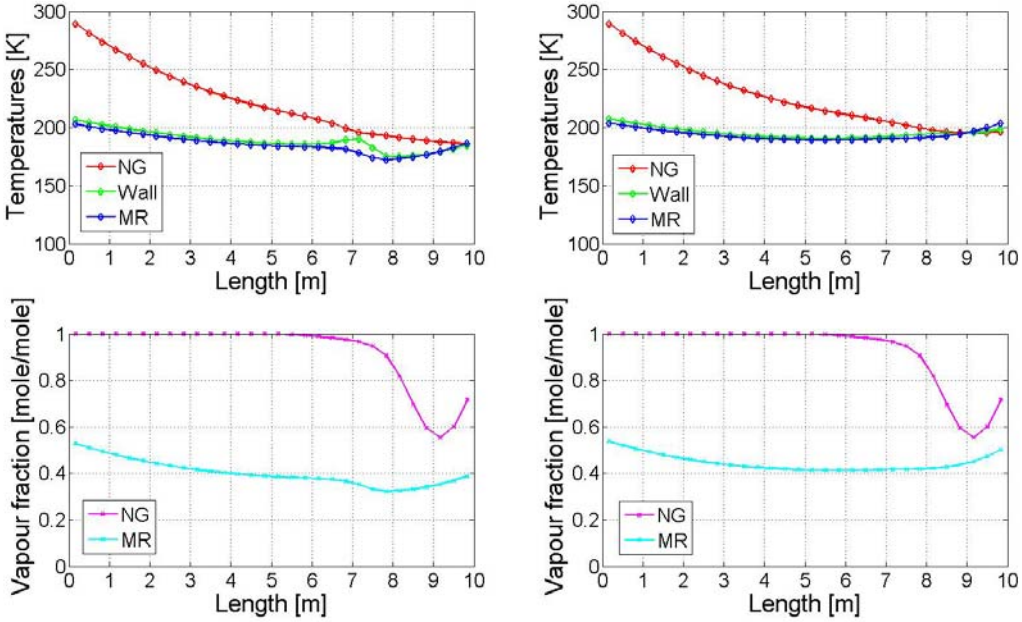

Temperatures and vapour fractions at t=516s and at t=520s

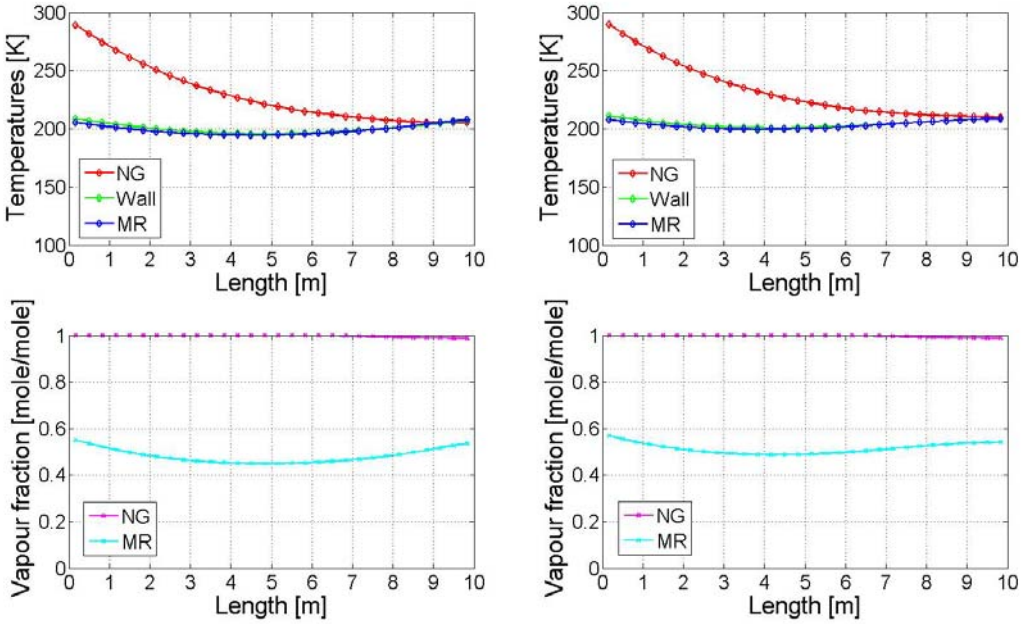

Temperatures and vapour fractions at t=524s and at t=528s

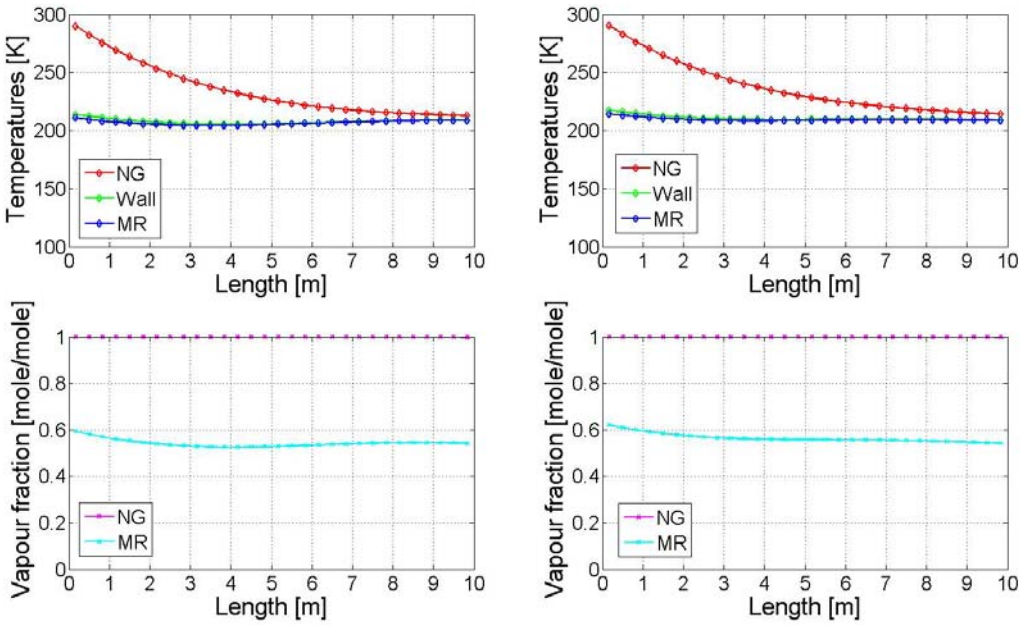

Temperatures and vapour fractions at t=532s and at t=536s

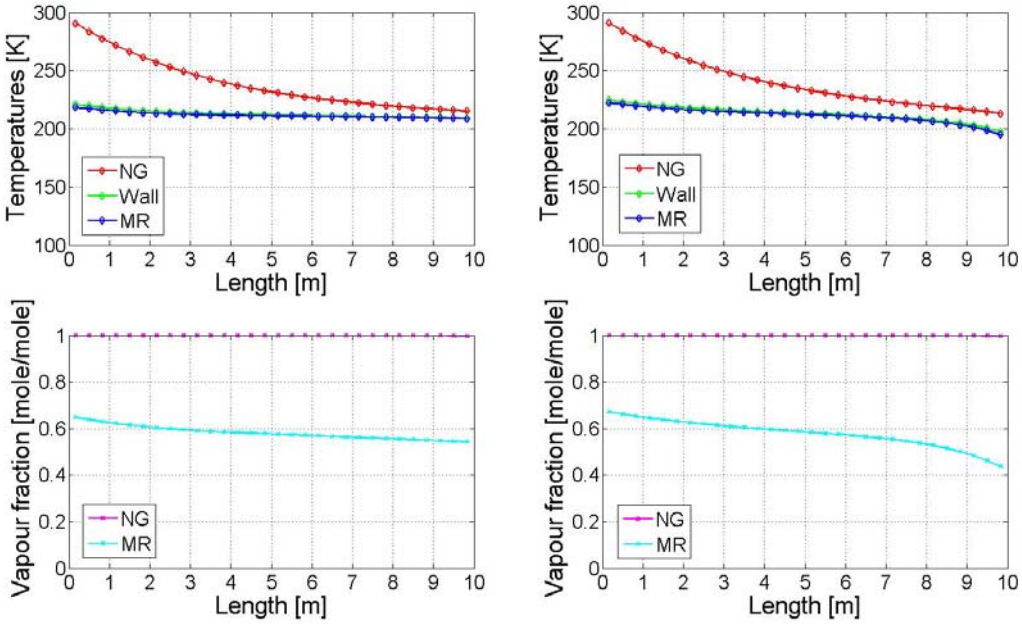

Temperatures and vapour fractions at t=540s and at t=544s

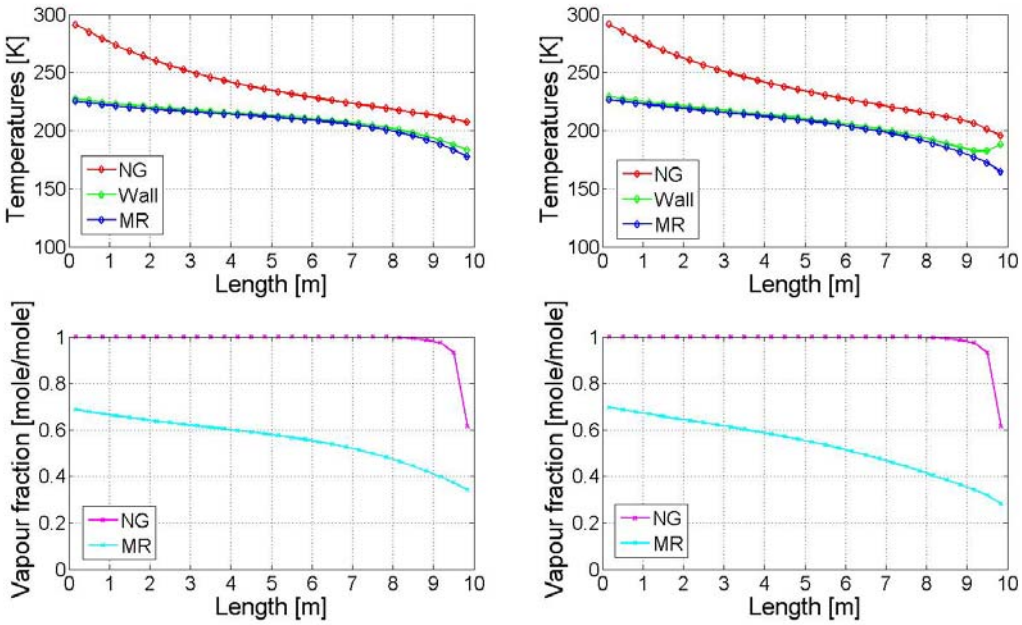

Temperatures and vapour fractions at t=548s and at t=552s

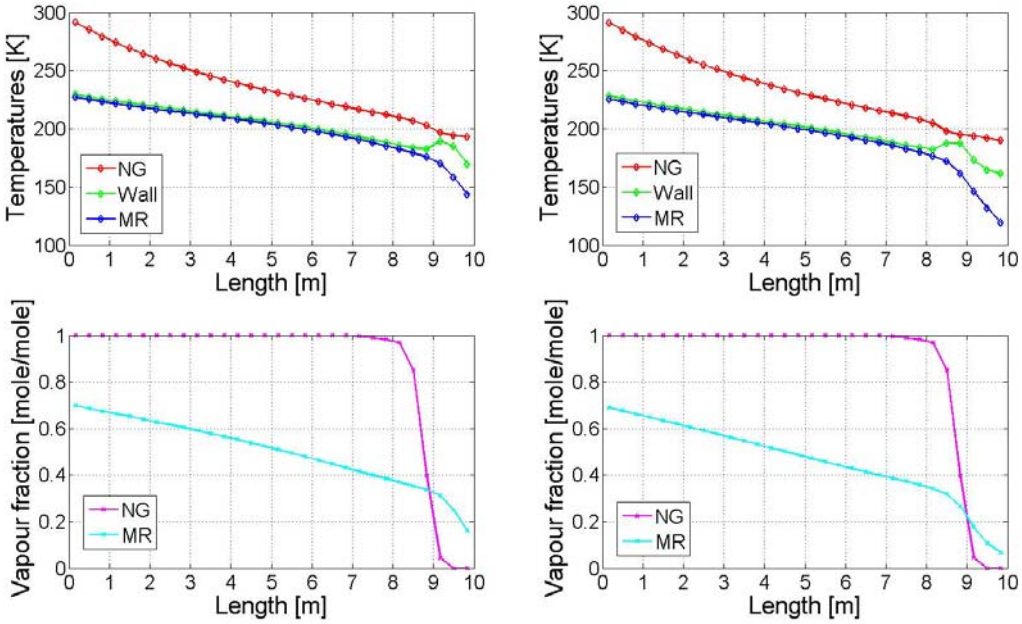

Temperatures and vapour fractions at t=556s and at t=560s

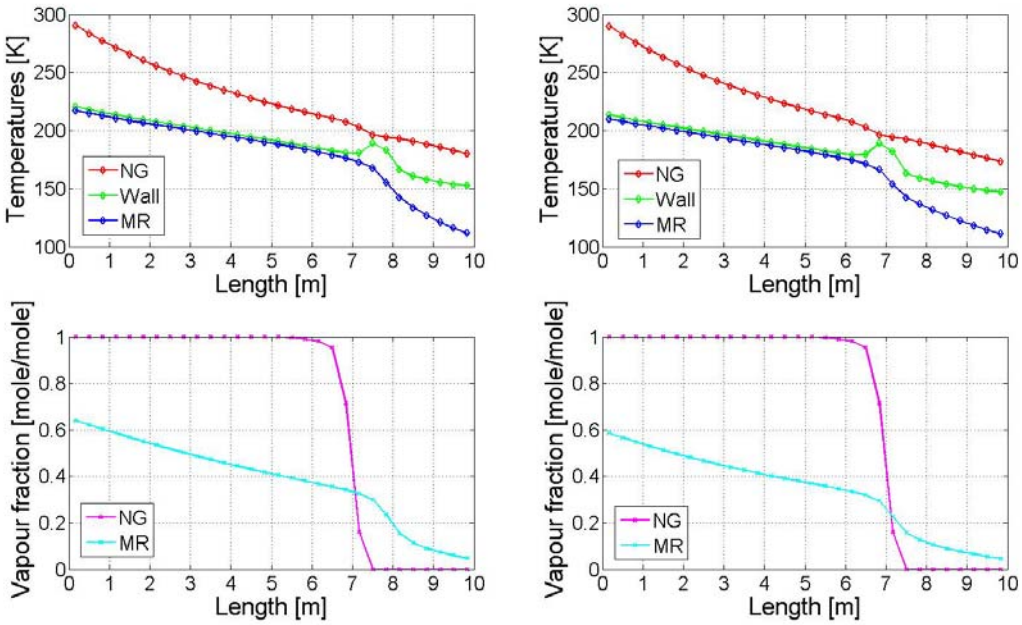

Temperatures and vapour fractions at t=570s and at t=580s

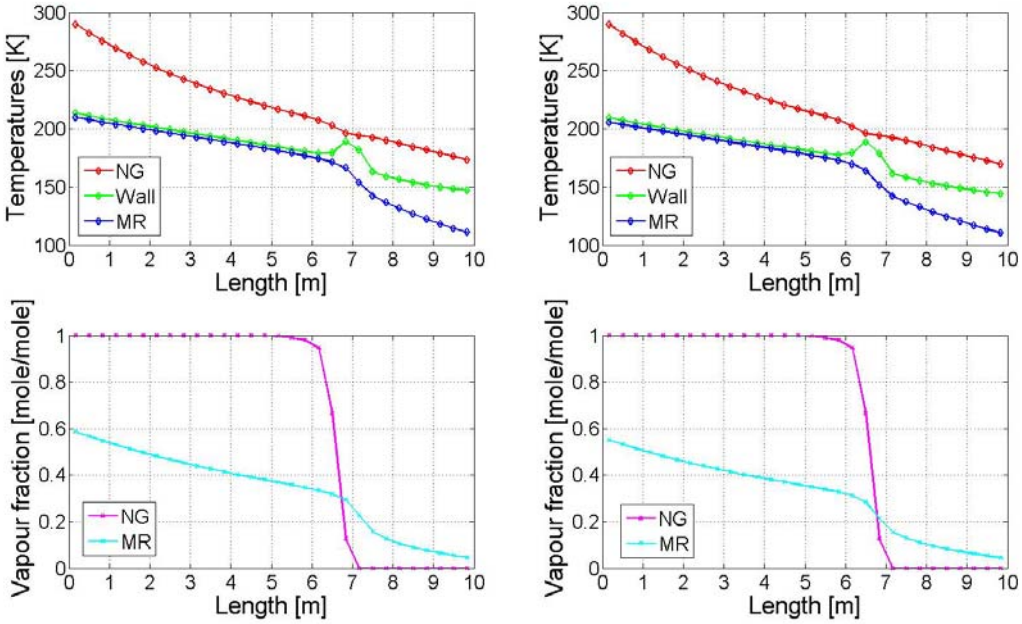

Temperatures and vapour fractions at t=590s and at t=600s